POLITECNICO DI MILANO
Dipartimento di Ingegneria Energetica

Synthesis of Carbon Nanotubes on Indium-Tin Oxide for Organic Solar Cells

Relatore interno: Prof. Luigi Pietro Maria Colombo
Relatore esterno: Prof. Nunzio Motta

Tesi di laurea di:
Michele Vedovati Matr.725307

Anno accademico 2009/2010

Ringraziamenti

Il primo ringraziamento va a mio padre, mia madre e mio fratello per essermi sempre stati accanto, per avermi incoraggiato e, quando serviva, criticato. Ringrazio anche tutta la mia famiglia che ha sempre dimostrato di avere fiducia nelle mie capacità.

Questo lavoro è stato possibile solo grazie al Professor Luigi Colombo, al Professor Nunzio Motta e all'Ingegner Andrea Capasso; mi hanno concesso un'occasione davvero unica e la loro soddisfazione nel leggere questa tesi è stata per me un gioia immensa.

Voglio ringraziare chi ha veramente creduto in me, chi mi ha voluto bene e chi mi ha amato; non ho bisogno di scrivere nessun nome perché chi leggerà queste righe saprà riconoscersi in tali sentimenti.

Si conclude così un capitolo della mia vita e il mio augurio più grande è quello di poter essere, oltre ad un buon ingegnere, un vero uomo.

Outline

Abstract

Carbon nanotubes (CNTs), tiny tubes made of carbon atoms are expected to become the ideal constituent of many technologies, in particular for future generation electronics. CNTs present, amongst the others, several unique properties which make them ideal as building blocks for a new generation of electronic devices: radius in the nanometer range, length reaching millimeters, ballistic electron transport, super-high current-carrying capacity, very high mechanical strength. These superior characteristics make carbon nanotubes the most promising building block for electronic devices of the future.

In this project CNTs are grown on Indium-Tin Oxide (ITO) substrates in order to be used as transparent electrode for organic solar cells, also named Organic Photovoltaics (OPVs). OPVs based on a bulk heterojunction made of a conductive polymer mixed to a carbon nanostructure offer potential advantages compared to conventional inorganic cells, like low costs, lightweight and flexibility. Recently CNTs have been proposed to increase the efficiency of the cells, by quickly collecting the electrons generated by the light.

The aim of this work is to create a nanotube carpet on ITO substrate to provide a transparent electrode for the solar cells. At present, the most promising method in order to synthesize CNTs is Chemical Vapor Deposition (CVD), which provides large density and high purity CNT carpets on different substrates. This method provides a high degree of control over the morphology and structure of the CNTs by a careful choice of catalyst particle size and growth conditions. Even though CVD is a valid method for extensive CNTs growths, a major problems still affects its performance. Actually the effect of some parameters that remain unpredictable prevents the exact control on the position and structure of the single nanotube. To effectively control the CNTs growth a complete knowledge of the growth mechanism is required.

To find the optimum synthesis technique in order to grow CNTs on ITO substrates, our experimental procedure have been repeated by changing the following parameters: Ni vs Fe as catalysts; thickness of the catalyst layer (5 to 20 nm); gas mixtures (Acetylene and Acetylene plus Hydrogen); flow rates (15 – 150 sccm); growth temperature (500 - 600°C); growth time (10 to 30 minutes).

After several attempts we have been able to select the best conditions for the growth of short nanotubes with the desired density on ITO substrates, as shown by Scanning Electron Microscope (SEM) images. Optical transmission measurements and electrical characterisation of a solar cell realised with this

CNTs-ITO substrate confirm that the presence of CNTs can improve the efficiency of the organic solar cell.

Key words: Carbon Nanotubes (CNTs), Organic Photovoltaic (OPV) cell, Chemical Vapor Deposition (CVD), Indium-Tin Oxide (ITO), CNTs Growth, efficiency.

Sommario

I nanotubi in carbonio (CNTs), minuscoli tubi composti da atomi di carbonio, potrebbero essere l'elemento ideale per molte tecnologie, in particolare per future applicazioni elettroniche. I CNTs in carbonio presentano, tra molte, caratteristiche uniche che li rendono il blocco principale per una nuova generazione di dispositivi elettronici: un raggio nell'ordine dei nanometri, altezze nell'ordine dei millimetri, un trasporto balistico dell'elettrone, grande capacità di trasporto della corrente elettrica, elevata forza meccanica. Queste caratteristiche superiori rendono i CNTs in carbonio una promessa come blocco costitutivo nelle generazioni future di per i dispositivi elettronici.

In questo progetto i CNTs in carbonio sono cresciuti su un substrato composto da ossido di indio e stagno (ITO) in modo da esser utilizzati come elettrodo trasparente per le celle solari organiche, dette anche celle fotovoltaiche organiche. Tali celle si basano su una giunzione detta bulk heterojunction e sono composte da polimeri conduttori misti ad una struttura di CNTs in carbonio; offrono vantaggi potenziali se comparati alle classiche celle inorganiche quali bassi costi, peso leggero, e flessibilità. Recentemente i CNTs in carbonio sono stati proposti per incrementare l'efficienza delle cella, dovuto al rapido collezionamento di elettroni una volta assorbita la luce.

Lo scopo di questo progetto è la creazione di un tappeto di CNTs su un substrato di ITO per fornire l'elettrodo trasparente alle celle solari. In questo momento, il metodo più promettente per la sintesi dei CNTs è la tecnica detta Chemical Vapor Deposition (CVD) che permette alta densità e un elevato grado di purezza dei tappeti di CNTs nei vari substrati. Questo metodo permette un elevato grado di controllo sulla morfologia e strutture dei CNTs grazie ad una attenta scelta della deposizione del catalizzatore e delle condizioni di crescita. Sebbene la CVD sia un metodo valido per la crescita dei CNTs, un grande problema influenza ancora le perfomance di tale tecnica. Esso è rappresentato dall'effetto di alcuni parametri che rimane ancora imprevedibile impedendo l'esatto controllo della posizione e della strutture del singolo nanotubo. Per controllare effettivamente la crescita dei CNTs è necessaria una conoscenza del meccanismo di crescita.

Per ottenere la sintesi perfetta di CNTs sui differenti substrati di ITO, le nostre procedure sperimentali sono state ripetute cambiando i seguenti parametri: Ni vs Fe come catalizzatori; spessore del catalizzatore depositato (dai 5 ai 20nm); gas utilizzati (Acetilene, Idrogeno); flusso di gas (15-150 sccm); temperatura per la crescita (dai 500 ai 600 °C); tempo di crescita (10-30 minuti).

Dopo diverse prove siamo stati in grado di selezionare le migliori condizioni per la crescita di nanotubi con opportune altezze e desiderate densità sui substrati di ITO, come mostrato dalle immagini dello Scanning Electron Microscope (SEM). La misura della capacità ottica e la caratterizzazione elettrica della cella solare realizzata con il substrato di ITO-CNTs confermano che la presenza di CNTs può migliorare l'efficienza della cella solare organica.

Parole chiave: Nanotubi in carbonio (CNTs), Fotovoltaico Organico (OPV), Chemical Vapor Deposition (CVD), Ossido di indio e stagno (ITO), crescita di CNTs, efficienza.

Table of Figures

List of Tables

Terminology

EIA: Energy Information Administration;
PV: Solar Photovolaic;
R&D: Research and Development;
PCEs: Power Conversion Efficiencies;
DSSC: Dye Sensitized Solar Cells;
OPVs: Organic Photovoltaics;
P3HT:Poly(3-hexylthiopen);
CNTs: Carbon Nanotubes;
PEDOT:PSS: poly(3,4-ethy;enedioxythiophene):poly(styrene sulfonate);
ITO: Indium-Tin Oxide;
MWCNTs: Multi-Walled CNTs;
SWCNTs: Single-Walled CNTs;
DWNT: Double-Walled CNTs;
CVD: Chemical Vapor Deposition;
HRTEM: High-Resolution Transmission Electron Microscopy;
SEM: Scanning Electron Microscopy;
MO: Molecular Orbital
HOMO: Highest Occupied Molecular Orbital;
LUMO: Lowest Unoccupied Molecular Orbital;
LED: for Light Emitting Diodes;
VA-CNTs: vertically-aligned carbon nanotubes;
FIB: Focused Ion Beam.

“Tutti i grandi sono stati piccoli, ma pochi di essi se ne ricordano.”

"Il piccolo principe", Antoine Marie Roger de Saint Exupèry

1 INTRODUCTION

1.1 WORLD ENERGY DEMAND

The continuous growth of energy demand has brought science to search for new energy sources and for new conversion processes in order to maximize the energy availability to the community. According to Energy Information Administration's International Outlook 2009 [1], the world energy demand is rapidly rising after year, as shown in Figure 1.1(a). If the figures of 2006 are considered, according to predicted values, by 2030 a 44% rise of world energy consumption over 2006 levels is projected. Despite the world's concern about greenhouse gases and pollution, most of the energy to fulfill the worldwide demand today and into the near future will be provided by liquid fuels, with a sizeable increase of projected utilization values for coal and renewable sources. This trend is reported in Figure 1.1(b).

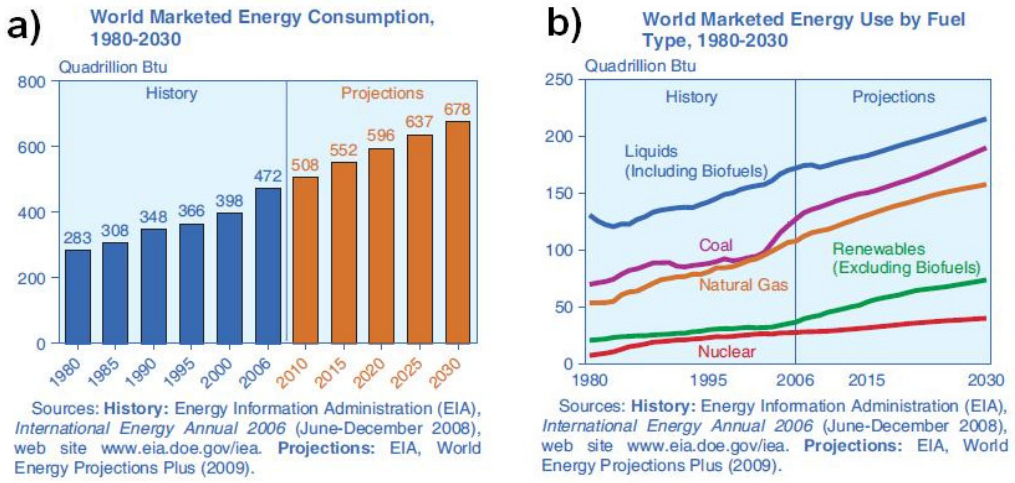

Figure 1.1. a) World marketed energy consumption and projection according to Energy Information Administration (EIA), b) World energy use generation by fuel [1].

Electric energy is expected to provide an increasing quota of the world's total energy demand and it is recognized as the fastest-growing form of end-use energy.

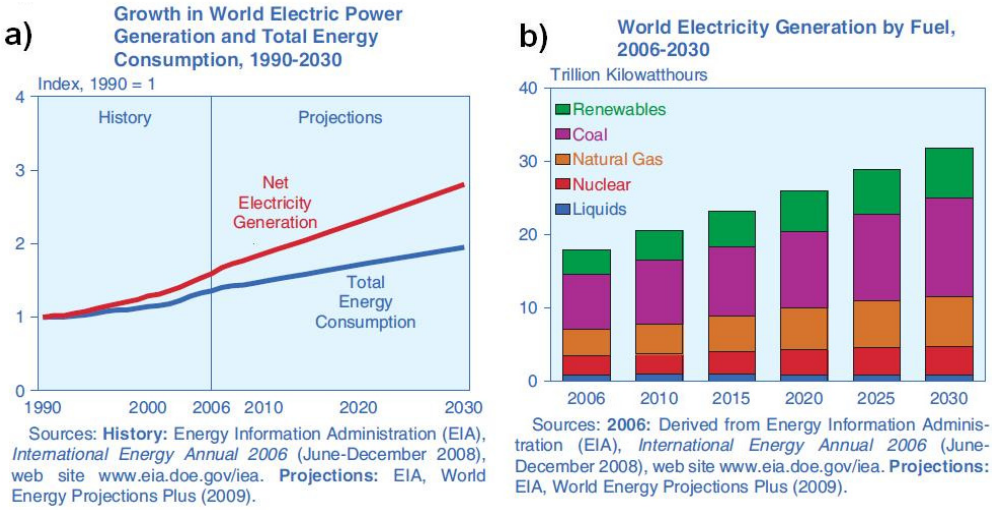

Figure 1.2. a) World electric power generation compared to total Energy consumption, b) World electricity generation by fuel [1].

In fact, as reported in Figure 1.2(a), the growth rate of electricity generated expected to increase at a higher than energy consumption. Unfortunately the electricity is mostly generated by fuel and most of the electric energy utilized today is provided by coal, as shown in Figure 1.2 (b), creating increasing amount of greenhouse gases. This situation is believed to last for the next two decades; very interesting, for a better understanding of the growth of the primary energy demand, is the lecture presented by Professor Yogi Goswami from University of South Florida. In this report he figures out, on a low estimate of 2% average annual growth, that the primary energy request would be double by 2040 and triple by 2060. Resting on a mathematical and statistic model, he traces out a deadline for every non-renewable energy sources as natural gas, oil, nuclear power and coal as shown in Figure 1.3 (a), (b), (c), (d).

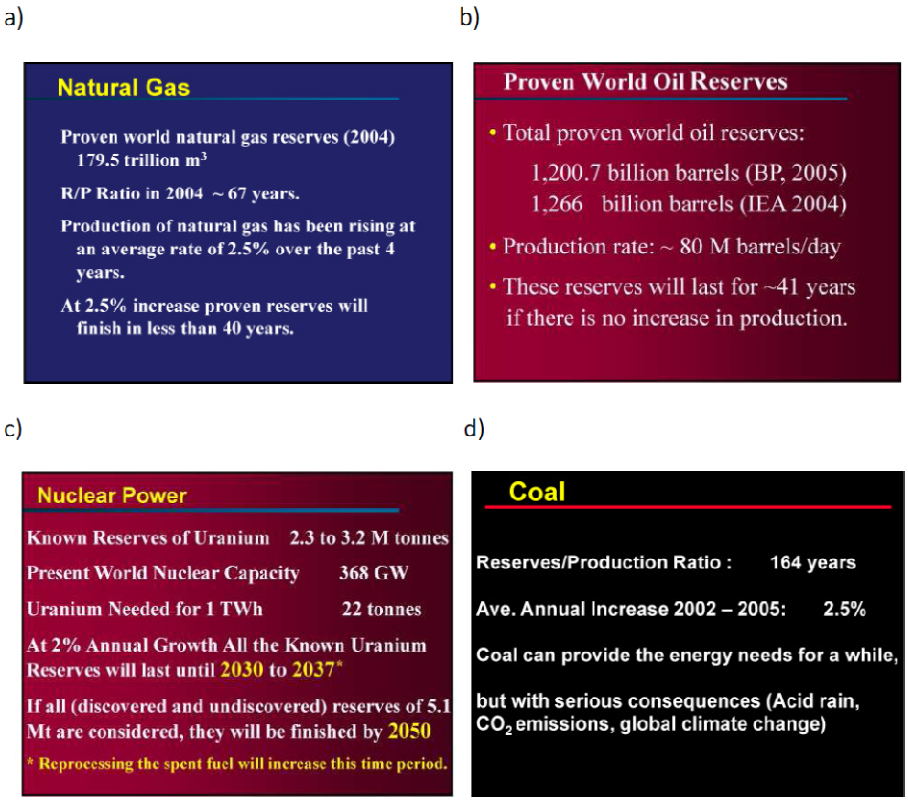

Figure 1.3. a) Estimate deadline for natural gas, b) Estimate deadline for oil reserves, c) Estimate deadline for nuclear power, d) Estimate deadline for coal production [4].

Although Figure 1.2(b) shows that the employment of renewable sources will increase, most of the electricity produced to meet the total energy demand, will continue to be provided by fossil-fuel sources. A clear example of this trend is graphed in Figure 1.4 for U.S.A. which highlights that only 7% of total energy is provided by renewable sources.

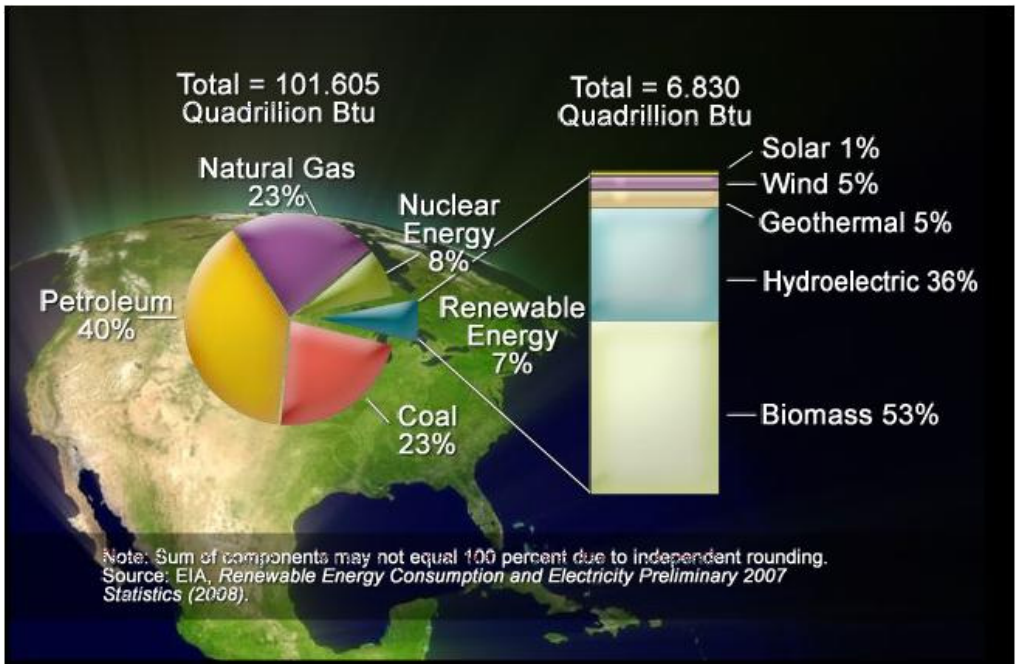

Figure 1.4. U.S.A. energy consumption quotes provided for different energy sources [1].

It is also interesting to note that among all sources of renewable energy, solar energy contributes only a 1% share to total energy supply. In general, renewable energy sources are considered expensive and capital-intensive, which present significant barriers to their implementation, with the natural resources needed that are typically located in remote areas. This last condition represents a disadvantage for an alternative way to produce energy on a large scale, can promote the local development of renewable energy sites, by eliminating the expensive energy delivery from the power grid. For example, for remote and sunny areas in countries like Italy, Spain or California, solar power can be more convenient than conventional power provided from the national grid. Alternatively, Government incentives represented by high feed-in retail tariffs (like in Germany or Japan) can lead to an increase of solar panel installation by end-users. Several studies report that renewable sources based on solar power efficient conversion into different types of energy (biomass fuel, water to hydrogen conversion, photovoltaics, etc) could be able to fully solve the planet's energy demand problem [2,3]. In relation to the renewable energies, an interesting result has been obtained by Solar Photovoltaics (PV): the cost decrease per Watt produced thanks to this technology. As a matter of fact the price has dropped from $100/W in the 1970s to 1.20$/W in 2010 and it is expected to be reached the limit of cost reduction in PV cells based on the

current concepts of 1$/W in 2012[4]. Figure 1.5 represents all the historical process about Photovoltaic costs.

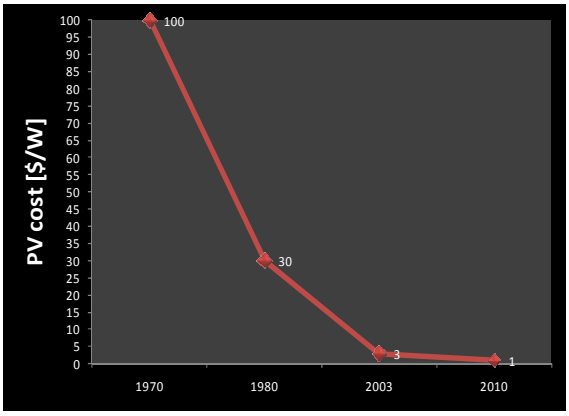

Figure 1.5. Photovoltaic costs decrease in the last 40 years, expressed in $/W.

An important alternative in renewable energies is given by Biomass that in 2050 could equal total world primary energy use today. To date, the 11% of world energy today comes from Biomass; however it is only 18% of what could be [4]. In Figure 1.6 shows the increase of Biomass (expressed in Million Liters) starting from 1975.

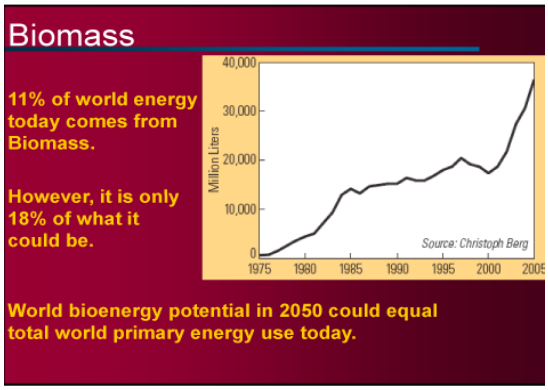

Figure 1.6. Photovoltaic costs decrease in the last 40 years, expressed in $/W [4]

The previous considerations about the world energy situation, the annual growth of primary energy demand and the prevision of the end of the current primary energy sources as oil, carbon, natural gas and nuclear power strictly must make

us consider renewable energies as providers of our energy[4]. As suggested by Professor Gosmani, Renewable Energy will have to give to the world at least 50% of our energy by 2050. For this reason is very important that R&D (Research and Development) must be accelerated, and policies necessary to push the market towards the "right" direction must be adopted without any delay to achieve the goal.

1.2 SOLAR ENERGY AND PHOTOVOLTAICS

Solar energy can be assumed as an endless source and so can be considered an excellent "renewable" energy resource. In one hour, the Sun delivers more energy to the Earth (4.3×10^{20}J) than all the energy consumed on the planet in a year (4.1×10^{20}J) [5]. Converting only 0.01% of this energy into usable forms could solve most of the energy needs of humanity for the next centuries with reduced damage to the environment through limited, or zero emission of greenhouse gases.

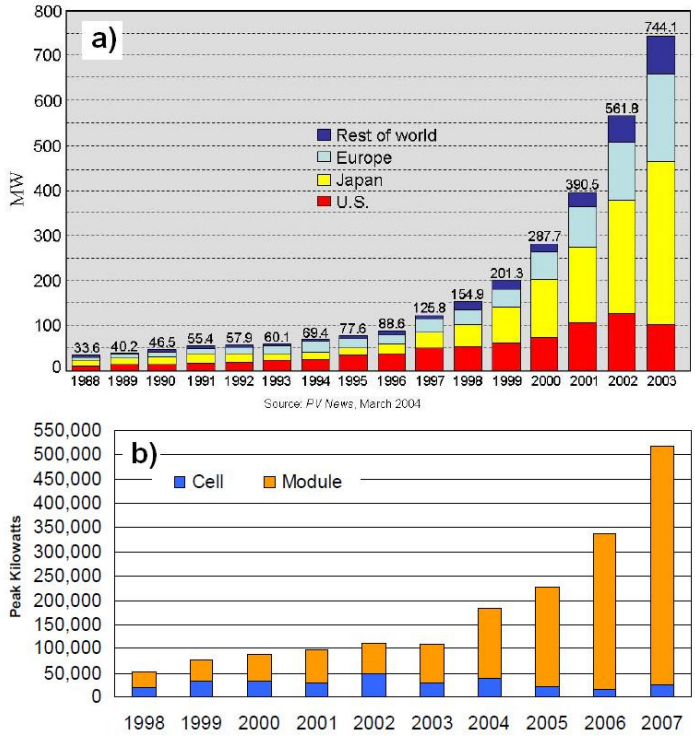

Figure 1.7. a) World photovoltaic and cell/mobile annual production [2], b) U.S.A. cell/module annual production [6].

As reported in the previous paragraph, electricity represents the fastest growing way to provide energy and "photovoltaics" directly convert solar energy into electricity. Unfortunately, to date only 0.1% of the world's electricity is supplied by photovoltaic devices [5]. Nevertheless,as depicted in figure 1.7, the annual production of photovoltaic cells and module, both in the world and in U.S.A., is increasing, representing a rising quota of electricity energy provided directly from the sun.

At present, commercial photovoltaic market is dominated by the inorganic multi-crystalline silicon solar cells. Even if these inorganic photovoltaic cells are a cheap and environmentally benign alternative to the full-blown plants, like other renewable energy options they are too expensive to be implemented. This is due to a series of energy intensive fabrication processes which requires high temperatures and a vacuumed environment to obtain a high purification level of silicon. Therefore, to effectively and economically utilize sunlight for the energy needs of humanity, photovoltaic cells with lower fabrication costs in largescale applications are needed.

A possible way to face the above mentioned drawbacks is by developing photovoltaic cells from materials which can be processed as easily as plastic and have high potential for low cost solar energy : Organic solar cells.

1.3 INORGANIC SEMICONDUCTOR PHOTOVOLTAICS

The greatest photovoltaic market supply is today provided by silicon solar cells and modules, with a quota higher than 90% of the total photovoltaic output from all sources [7]. This huge share of the photovoltaic market is believed to be strongly reduced in the future for several reasons. First, at this growth rate, a silicon shortage is expected to strike the world market [8]. Second, new generation photovoltaic technologies like thin film solar cells and organic solar cells are expected to be extremely cheap, providing a replacement to the comparatively high-cost silicon devices. Finally, it must be noted that other technologies have already reached power conversion efficiencies (PCEs) comparable or higher than silicon ones, as reported in Figure 1.8.

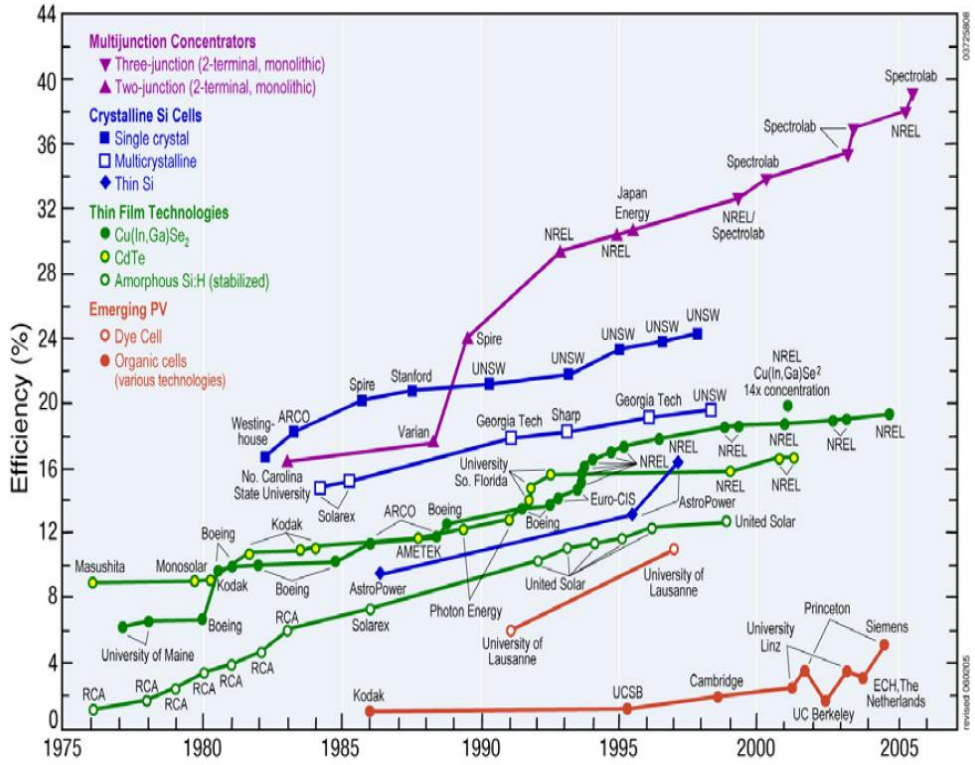

Figure 1.8. Improvements of solar cells efficiences for different semiconductors [2].

As could be expected, high PCEs can help to lower the price of solar cells and modules, rising up the market penetration of photovoltaic devices. In fact, despite silica being relatively cheap and abundant on the Earth surface, the expensiveness of silicon technology is due to the purification processes needed to produce high quality devices. The right way to evaluate the cost of a photovoltaic technology is to calculate the cost-per-watt-peak ($/$W_p$ or €/W_p) figure of merit. It corresponds to the ratio of the module cost per unit area ($/$m^2$ or €/m^2) divided by the maximum electric power delivered per unit area (when illuminated by 1000 W/m^2, the peak power from the sun for standard evaluation). Taking into account all the additional costs and the average availability of solar irradiance, the cost-per-watt-peak can be related to the cost per kilowatt-hour according to relationship 1 $/$W_p$ – 0.05 $/kWh, even though alternative values could be provided for different geographical locations. Although the cost-per-watt-peak dropped from around 70 $/$W_p$ in the 1970s to today's cost around 4-5 $/$W_p$, the value of 0.4 $/$W_p$ is considered the final goal for massive implementation of photovoltaic modules in energy infrastructures [2].

The viability of conventional silicon photovoltaic technology as a solution to provide energy for the world's increasing energy demands, has been often challenged from an energetic point of view [9] based on the argument that energy required to build a silicon solar cell is higher than the energy produced by the same device during its lifetime. Several studies [10, 11] have been conducted to calculate the net energy payback period for several kinds of silicon solar cells. In standard operating conditions and in the worst case, within five years the photovoltaic device will have paid back for the energy required to build it [12].

Therefore, although there are still many open problems regarding this technology, the second most abundant element on the Earth's crust can be considered extremely attractive as a major source of energy and during its thirty-year lifetime, silicon solar cells will produce between 6 and 31 times the amount of energy used to build them.

1.3.1 **SOLAR CELLS BASIC PRINCIPLES**

A photovoltaic device is capable of supplying electric power to a load connected to it once it is exposed to sunlight, directly converting the energy from light to electricity.

Most photovoltaic devices are based on the *pn* junction principle. According to this, two different regions can be indentified within the active media absorbing the light, denominated *n* and *p* as they contain an excess of electrons or holes respectively due to impurities. As depicted in Figure 1.9(a), the regions *n* and *p* have two different Fermi energy levels that must coincide at thermodynamic equilibrium. Therefore, if the two regions interact, charge migration occurs across the *pn* junction. As a consequence of the double layer of ions left behind by the moving charges, an electric field $\boldsymbol{\varepsilon}_F$ is established; the equilibrium is reached when the two Fermi levels are equal.

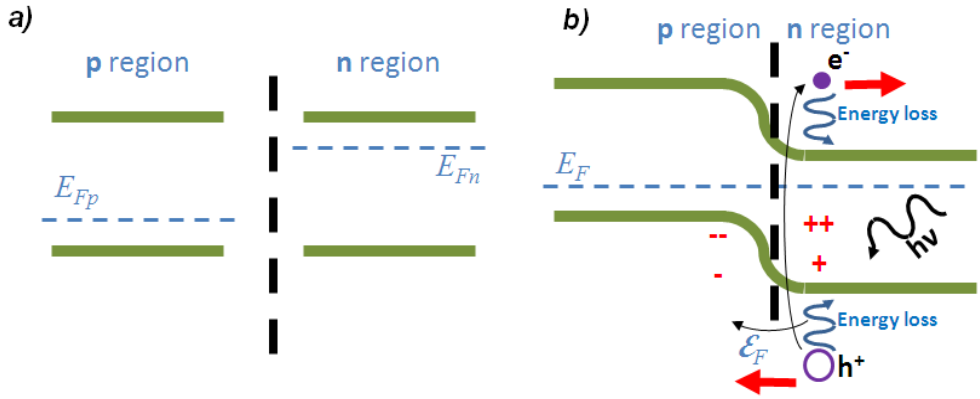

Figure 1.9. a) Isolated n and p materials. b) Photovoltaic generation in pn junction solar cell.

As depicted in Figure 1.9(b), when the photon is absorbed an electron-hole pair is generated and the electric field acts in the opposite direction to each charge, contributing to charge separation and collection. Even if the charges have a high energy upon absorption, thermal decay occurs and transport takes place at the material's energy band minimum. As can be observed, the energy of the photon needed to create an electron-hole pair must be higher than the energy gap in the energy density of states available for electrons. Radiation with energy lower than the gap cannot be absorbed by the medium and no photovoltaic effect can be generated. Today, research on solar cells is focused on the materials with an energy gap matched to the solar spectrum (1.4-1.8 eV) [13] or built with multiple *pn* junctions. In this way, most of the photon wavelengths in the sun spectrum can be harvested and, at the same time, electrons and holes can be transported with limited energy loss.

1.3.2 PERFORMANCE OF PHOTOVOLTAIC DEVICES

The performance of a solar cell is evaluated according to the typical current-voltage curve response, reported in Figure 1.10, which shows the behavior of the device in the dark and when exposed to sunlight.

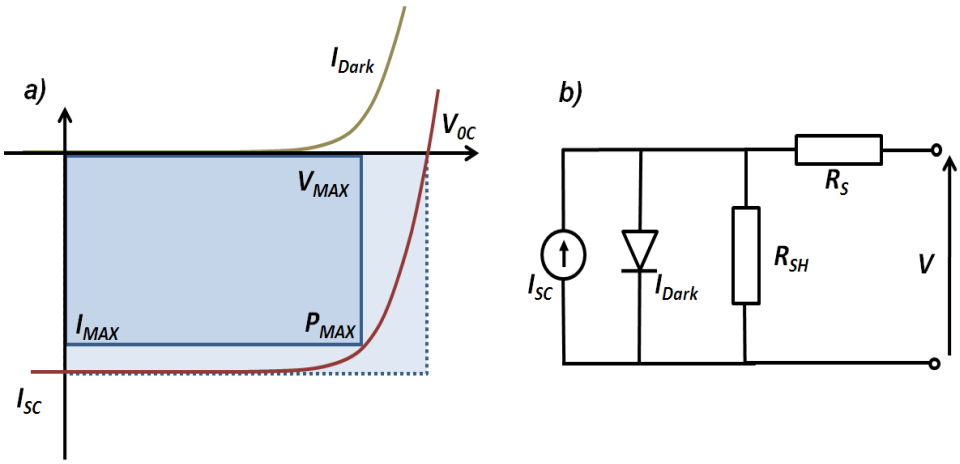

Figure 1.10. a) Solar cell performance curve. b) Solar cell equivalent circuit

When exposed to sun light the solar cell shows the same characterist shifted vertically into the fourth quadrant of the I vs V graph and hence generates power. If the device is short circuited the current generated, namely I_{SC}, is the highest possible, whereas, when the circuit is opened the highest output voltage V_{OC} is present at the terminals of the solar cell.

Over the range of all voltage-current values in the performance curve of Figure 1.10(a), it is possible to identify I_{MAX} and V_{MAX}, which corresponds to the maximum power P_{MAX} generated by the device. The power conversion η (or PCE) of the solar cell can therefore be defined by the ratio of the maximum power generated divided by the incident power P_I as follows:

$$\eta = \frac{P_{MAX}}{P_I} = \frac{V_{MAX} * I_{MAX}}{P_I} = \frac{V_{OC} * I_{SC} * FF}{P_I} \tag{1.1}$$

Where FF is the fill factor of the solar cell, defined as the ratio of the product $I_{SC}V_{OC}$ divided by $I_{MAX}V_{MAX}$. The fill factor takes into account non-ideality factors that affect the performance of the solar cell. Non-ideal behaviour is typically modelled with the presence of a shunt resistance R_{SH} and a series resistance R_s in the device's equivalent circuit as reported in Figure 1.10(b). The reduction of the fill factor, as a result of the increase of the series resistance or

the decrease of the shunt resistance increase, is shown in Figure 1.11(a) and (b) respectively. In these examples the values of I_{SC} and V_{OC} are kept constant to show the effect of each resistance on the same device.

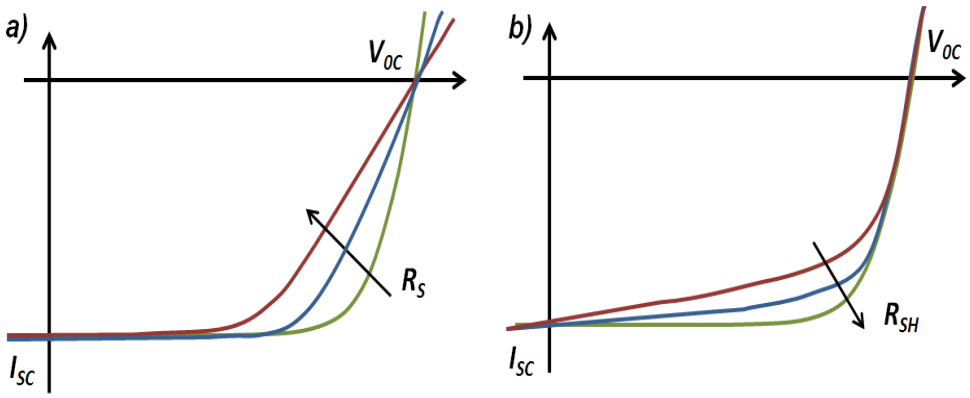

Figure 1.11. Effect on the solar cell performance as the value of series resistance RS is increased (a) or as the value of shunt resistance RSH is reduced (b).

1.3.3 SOLAR CELLS AND STATE OF THE ART

Photovoltaic technologies and devices are among the most studied topics in the scientific literature and new studies regarding achieved results and novel technologies are published continuously. Periodically, in a dedicated publication, the highest power conversion efficiencies are reported for each kind of device type, classified accordingly to the active media converting the energy [14]. The following Figure 1.12 reports the highest power conversion efficiencies of solar cells based on a variety of different technologies.

Classification[a]	Effic.[b] (%)	Area[c] (cm^2)	V_{oc} (V)	J_{sc} (mA/cm^2)	FF[d] (%)	Test centre[e] (and date)	Description
Silicon							
Si (crystalline)	**25.0 ± 0.5**	4.00 (da)	0.705	**42.7**	82.8	Sandia (3/99)[f]	UNSW PERL[12]
Si (multicrystalline)	**20.4 ± 0.5**	1.002 (ap)	0.664	**38.0**	80.9	NREL (5/04)[f]	FhG-ISE[13]
Si (thin film transfer)	**16.7 ± 0.4**	4.017 (ap)	0.645	**33.0**	78.2	FhG-ISE (7/01)[f]	U. Stuttgart (45 μm thick)[14]
Si (thin film submodule)	**10.5 ± 0.3**	94.0 (ap)	0.492[g]	**29.7**[g]	72.1	FhG-ISE (8/07)[f]	CSG Solar (1-2 μm on glass; 20 cells)[15]
III-V cells							
GaAs (crystalline)	**26.1 ± 0.8**	0.998 (ap)	1.038	**29.7**	84.7	FhG-ISE (12/07)[f]	Radboud U. Nijmegen[6]
GaAs (thin film)	**26.1 ± 0.8**	**1.001 (ap)**	**1.045**	**29.5**	**84.6**	**FhG-ISE (07/08)[f]**	**Radboud U. Nijmegen[6]**
GaAs (multicrystalline)	**18.4 ± 0.5**	4.011 (t)	0.994	**23.2**	79.7	NREL (11/95)[f]	RTI, Ge substrate[16]
InP (crystalline)	**22.1 ± 0.7**	4.02 (t)	0.878	**29.5**	85.4	NREL (4/90)[f]	Spire, epitaxial[17]
Thin film chalcogenide							
CIGS (cell)	**19.4 ± 0.6**[h]	0.994 (ap)	0.716	**33.7**	80.3	NREL (1/08)[f]	NREL, CIGS on glass[18]
CIGS (submodule)	**16.7 ± 0.4**	16.0 (ap)	0.661[g]	**33.6**[g]	75.1	FhG-ISE (3/00)[f]	U. Uppsala, 4 serial cells[19]
CdTe (cell)	**16.7 ± 0.5**[h]	1.032 (ap)	0.845	**26.1**	75.5	NREL (9/01)[f]	NREL, mesa on glass[20]
Amorphous/nanocrystalline Si							
Si (amorphous)	9.5 ± 0.3[i]	1.070 (ap)	0.859	17.5	63.0	NREL (4/03)[f]	U. Neuchatel[21]
Si (nanocrystalline)	10.1 ± 0.2[j]	1.199 (ap)	0.539	24.4	76.6	JQA (12/97)	Kaneka (2 μm on glass)[22]
Photochemical							
Dye sensitised	10.4 ± 0.3[k]	1.004 (ap)	0.729	**22.0**	65.2	AIST (8/05)[f]	Sharp[23]
Dye sensitised (submodule)	8.2 ± 0.3[k]	25.45 (ap)	**0.705**[g]	**19.1**[g]	61.1	AIST (12/07)[f]	Sharp, 9 serial cells[24]
Dye sensitised (submodule)	8.2 ± 0.3[k]	18.50	0.659[g]	**19.9**[g]	62.9	AIST (6/08)[f]	Sony, 8 serial cells[25]
Organic							
Organic polymer	5.15 ± 0.3[k]	1.021 (ap)	0.876	**9.39**	62.5	NREL (12/06)[f]	Konarka[26]
Organic (submodule)	1.1 ± 0.3[k]	232.8 (ap)	29.3	0.072	51.2	NREL (3/08)[f]	Plextronics (P3HT/PCBM)[27]
Multijunction devices							
GaInP/GaAs/Ge	32.0 ± 1.5[j]	3.989 (t)	2.622	14.37	85.0	NREL (1/03)	Spectrolab (monolithic)
GaInP/GaAs	30.3[j]	4.0 (t)	2.488	14.22	85.6	JQA (4/96)	Japan Energy (monolithic)[28]
GaAs/CIS (thin film)	25.8 ± 1.3[j]	4.00 (t)	—	—	—	NREL (11/89)	Kopin/Boeing (4 terminal)[29]
a-Si/μc-Si (thin submodule)[j,l]	11.7 ± 0.4[j,l]	14.23 (ap)	5.462	2.99	71.3	AIST (9/04)	Kaneka (thin film)[30]

Figure 1.12. Report of the latest certified best results for photovoltaic modules of different materials[14].

As it could be read from the table, silicon used in 3 forms (crystalline, multicrystalline and amorphous) attained a best efficiency of 25%. It must also be noted that Photochemical Dye Sensitized Solar Cells (DSSC), a relatively young type of solar cell devised by O'Regan and Graetzel in 1991 [15], have already reached efficiencies of more than 10%. The highest PCEs have been achieved by thin film ternary chalcogenide active materials or alternatively by multijunction devices based on multi-groups compound semiconductors such as GaAs, GaInP and InP.

It is important to note that in order to maintain uniformity in measurements the standard conditions to test solar cells is at temperature T=25C°. For the incident power, the spectrum must coincide with one of the global air mass (AM) spectra defined as follows. An air mass 0 spectrum (AM0) corresponds to the solar spectrum outside of the earth's atmosphere, whereas AM1.5 is the spectrum of the sun at a zenith angle of 48.19° when measured at sea-level on the Earth surface. The AM1.5 spectrum with an incident power of 1000 W/m^2 is

the standard used to test solar cell for terrestrial application. As can be seen in the following Figure 1.13, the conditions of testing may vary for example by using light concentrators to expose the devices up to 1000 Suns. This can bring to reach power concentrations efficiencies of more than 40% has shown in the following for multijunction photovoltaic devices.

Classification	Effic.[a] (%)	Area[b] (cm^2)	Intensity[c] (suns)	Test centre (and date)
Single cells				
GaAs	**28.2 ± 1.0**	0.203 (da)	**213**	Sandia (8/88)[d]
Si	27.6 ± 1.0	1.00 (da)	92	FhG-ISE (11/04)
CIGS (thin film)	**21.8 ± 1.5**[f]	0.102 (da)	14	NREL (2/01)[d]
Multijunction cells				
GaInP/GaAs/Ge (2-terminal)	40.7 ± 2.4[e]	0.267 (da)	240	NREL (9/06)
GaInP/GaAs/GaInAs (2-terminal)	**40.8 ± 2.4**[e,f]	**0.0976 (da)**	**140**	**NREL (7/08)**
Submodules				
GaInP/GaAs/Ge	27.0 ± 1.5[g]	34 (ap)	10	NREL (5/00)
Modules				
Si	**20.5 ± 0.8**[f]	1875 (ap)	**79**	Sandia (4/89)[d]
Notable exceptions				
GaAs/GaSb (4-terminal)	32.6 ± 1.7[g]	0.053 (da)	100	Sandia (10/89)[d]
InP/GaInAs (3-terminal)	**31.7 ± 1.6**[f]	0.063 (da)	50	NREL (8/90)[d]
GaInP/GaInAs (2-terminal)	30.2 ± 1.2[g]	0.1330 (da)	300	NREL/FhG-ISE (6/01)
GaAs (high concentration)	**26.6 ± 1.0**	0.203 (da)	1000	Sandia (8/88)[d]
Si (large area)	**21.7 ± 0.7**	20.0 (da)	11	Sandia (9/90)[d]

[a]Effic. = efficiency.
[b](da) = designated illumination area; (ap) = aperture area.
[c]One sun corresponds to direct irradiance of 1000 Wm^{-2}.
[d]Recalibrated from original measurement.
[e]Measured under a low aerosol optical depth spectrum similar to ASTM G-173-03 direct[5].
[f]Not measured at an external laboratory.

Figure 1.13 Lastest certified best results for photovoltaic modules of different materials for illumination greater than one Sun [14].

1.4 ORGANIC SOLAR CELLS

An organic solar cell is a photovoltaic cell that uses organic electronics for light absorption and charge transport. In these kinds of solar cells the active element is not an inorganic semiconductor but is made by organic materials.

The term “organic materials” means conductive organic polymers or small organic molecules utilized to convert solar energy into electric energy. This technology has been referred as Organic Photovoltaics (OPV). Although OPV devices can be based on a vast range of active materials, the study proposed here was focused on mixtures of Poly(3-hexylthiopen) (P3HT) and carbon nanotubes (CNTs).

Organic solar cells have a singular advantage over their inorganic counterparts of being cheaper to be manufactured. These devices do not require the high deposition temperatures or complex processing as required in inorganic devices, and they can be solution-processed[16]. Moreover, the conjugate

polymer materials used in these devices also offer more flexibility than the silicon crystal used in inorganic solar cells, which males the development of flexible thin film solar cell possible. Such flexible cells, it is proposed, could be used in countless ways, from handheld electronics to commercial power production.

Although these organic solar cells are cheaper to their inorganic counter parts in term of large area applications, they have yet to be commercially viable. This is due to the low exciton lengths, low charge carrier mobility and susceptibility to degradation in the organic materials used. The device low performances could be improved by working on the nano-scale morphology on the organic materials used. In many recent studies, Fullerenes [17] and CNTs [18] have been pointed out as a promising material to enhance the organic solar cells efficiencies.

To date, inorganic solar cells based on conventional semiconductor like silicon has successfully achieved excellent efficiencies of 26% and the development of inorganic thin-layer and multi-junction devices have also lead to even better performance. On the contrary, the most efficient organic photovoltaic cell based on bulk-heterojunction consists in a blend of polymer and fullerenes (P3HT/PCBM) operates at 4.4% efficiency under AM 1.5 solar illumination [19], even if other authors consider efficiency of 10% within reach.

It is possible to summarize the operation of this photovoltaic device in three consecutive fundamental steps:

- absorption of light;
- creation of separate charges at the donor acceptor interfaces;
- selective transport of the charges through the bulk of the device to the appropriate collecting electrodes.

An important pre-requisite for highly efficient conversion of photons into electrical current is that holes and electrons do not recombine before being swept out of the device into the external circuit. Important factors are given by a metastable photoinduced charge-separated state and high charge carrier mobilities. The conjugated polymer-fullerene blends present ultrafast photoinduced charge transfer and a subsequent rather slow recombination that it's a perfect match for the OPVs. Once the metastable charge-separated state is formed, the free charges are transported through the device by diffusion processes.

In the active layer of the device, positive carriers (holes) are transported through the conjugated polymer matrix and negative carriers (electrons) are transported by hopping between fullerene molecules.

For the device represented in Figure 1.14, known as Brabec's cell, accordingly to what mentioned before, the conductive glass contact is the anode, the active layer polymer is the hole-conductive material and the back metallic contact is the cathode. Typical materials involved in the building of solar cells are Indium Tin Oxide (In_2O_3:S, ITO) for the transparent anode contact, poly(3,4-ethy;enedioxythiophene):poly(styrene sulfonate) (PEDOT:PSS) as electron blocking layer and aluminium for the back cathode contact.

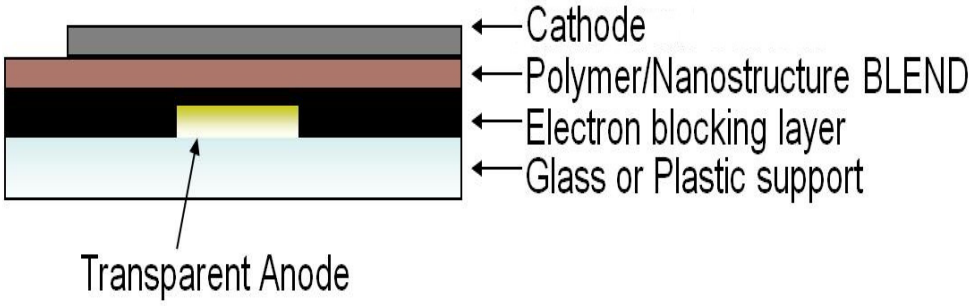

Figure 1.14 Ideal scheme of the organic solar cell.

1.5 PRESENT RESEARCH CHALLENGES

Low short circuit current density (J_{sc}) which is due to the limited ability of the photoactive material to efficiently absorb photons, dissociate excitons, and transport charge carriers to the respective electrodes have been pointed out as ones of the limiting factors that contribute to low power conversion efficiency in organic solar cells. In addition, disordered organic materials are widely known for their poor exciton diffusion lengths and low charge carrier mobilities, which seriously limit the J_{sc}. While issues on short exciton diffusion length had been largely solved by the introduction of bulk-heterojunction structures exhibiting nanoscale phase separation, the low charge carrier mobility still remains a limiting factor. The simplest means of overcoming this problem is to reduce the thickness of the active layer. Unfortunately, this approach reduces the optical absorbance resulting in a commensurate reduction in the light harvesting capability of the device. An alternative approach is the use of an interpenetrating

electrode that extends into the active organic layer, extracting charge carriers closer to the point of generation.

For the past decade, CNTs have been identified as the one of the most promising route in realizing high area, interpenetrating electrodes in organic solar cells. Multi-Walled CNTs (MWCNTs) confined to the donor layer of bi-layer photovoltaic cells have been utilized as the hole-extracting electrode [20, 21], where they have been shown to reduce the series resistance and increase fill factor of the device. On the other hand, Single-Walled CNTs (SWCNTs) have been utilized as the electron acceptor and electron-extracting electrode in heterojunction organic cells. Freestanding SWCNT films have also been demonstrated as a low cost alternative to indium tin oxide (ITO) glass in bulk heterojunction organic solar cells. This suggests that continuous films of high purity CNTs could be representative of a new class of transparent conducting materials with transparency and sheet resistance comparable to ITO.

The rationale of using this continuous array of vertically aligned CNTs is to minimize the distance to the junction without increasing the complexity of the path for the separated charges to travel, hence increasing the efficiency of the device. In this work, the ideal organic photovoltaic devices proposed will be fabricated through a combination of a continuous vertically aligned CNTs network and a polymer/fullerene (P3HT/PCBM) blend.

1.6 **PURPOSE OF THE PRESENT PROJECT**

This section aims to properly select the CVD operative parameters in order to achieve the optimal CNTs length. Actually CNTs should penetrate the active layer as deep as possible to efficiently collect electrons, without keeping in contact with the electrode to avoid short circuit. The entire process can be summarized into 4 stages as shown in Figure 1.15:

- Substrate fabrication
- Active layer fabrication
- Deposition of the metal electrode
- Characterization of the solar cell

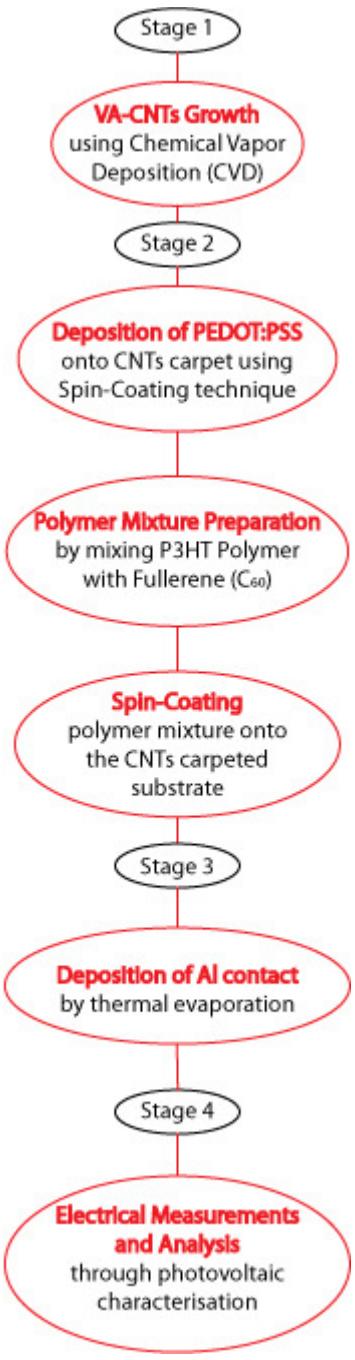

Figure 1.15 Block diagram on the overwiew of the fabrication processes and characterization involved in producing the organic photovoltaic cells.

2 SCIENTIFIC BACKGROUND

This chapter reviews the scientific background behind the project of this master research.

A brief presentation about carbon nanotubes is the first step. In order to achieve a better knowledge of the experiments, descriptions of CVD (chemical vapor deposition), growth mechanics, catalyst, inorganic photovoltaic cells, organic photovoltaic cells are given in this chapter.

2.1 CARBON NANOTUBES

2.1.1 INTRODUCTION

Carbon is the most versatile element in the periodic table, owing to the type, strength, and number of bonds it can form with many different elements. The existence of structural isomers and geometric isomers are enabled by the diversity of bonds and their corresponding geometries.

The properties of carbon are a direct consequence of the arrangement of electrons around the nucleus of the atom. There are six electrons in a carbon atom, shared evenly between the 1s, 2s, and 2p orbitals. Since the 2p atomic orbitals can hold up to six electrons, carbon can make up to four bonds; however, the valence electrons, involved in chemical bonding, occupy both the 2s and 2p orbitals. Covalent bonds are formed by promotion of the 2s electrons to one or more 2p orbitals; the resulting hybridized orbitals are the sum of the original orbitals. Depending on how many p orbitals are involved, this can happen in three different ways. In the first type of hybridization, the 2s orbital pairs with one of the 2p orbitals, forming two hybridized sp^1 orbitals in a linear geometry, separated by an angle of 180°. The second type of hybridization involves the 2s orbital hybridizing with two 2p orbitals; as a result, three sp^2 orbitals are formed. These are on the same plane separated by an angle of 120°. In the third hybridization, one 2s orbital hybridizes with the three 2p orbitals, yielding four sp^3 orbitals separated by an angle of 109.5°[22]. In all three cases,

the energy required to hybridize the atomic orbitals is given by the free energy coming from the formation of chemical bonds with other atoms.

Solid phase carbon can be found in different allotropic forms with diverse and sometimes opposite electrical, mechanical and physical properties. These allotropic forms are three, as shown in Figure 2.1 and in Figure 2.2 : graphite, diamond, buckminsterfullerene (Figure 2.1) and graphene (Figure 2.2).

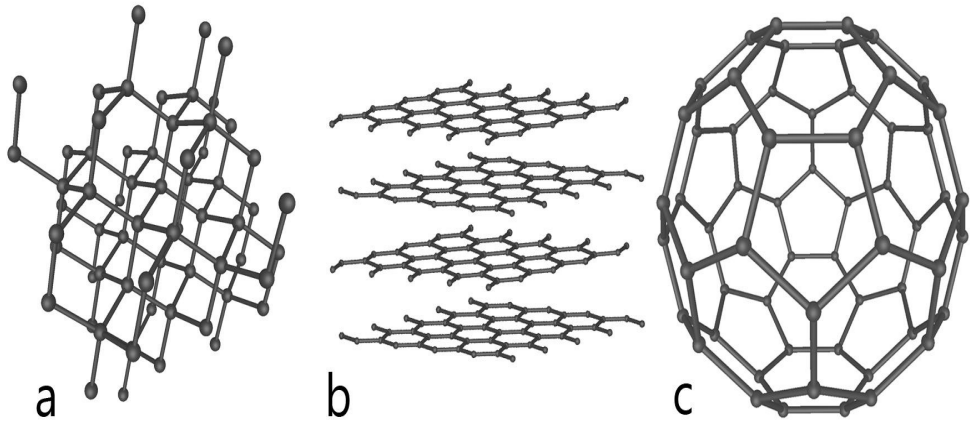

Figure 2.1. The three allotropes of carbon : a) Diamond, b) Graphite, c) Buckminsterfullerene [23].

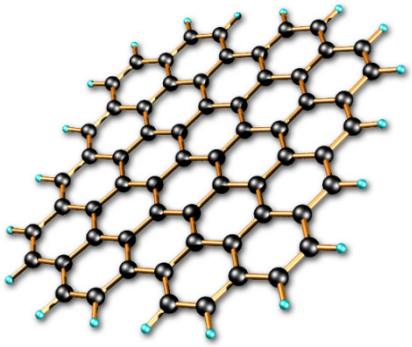

Figure 2.2. Graphene Sheet

In the diamond form, each sp^3 hybridized carbon atom is bonded to other four, in a perfect tetrahedral arrangement. The crystallinde network gives

diamond its hardness (it is the hardest substance known) and excellent heat conduction properties. The sp^3 hybridized bonds account for its electrically insulating property and optical transparency. Conversely, in the graphite form, the sp^2 atoms are organised in a planar layers and every atom is bonded to three others placed at 120°. The structure of each plane (referred as graphene) is like a honeycomb, where electrons can move freely from an unhybridized p orbital to another, forming an endless delocalized π bond network that gives rise to the electrical conductivity. Graphene is a flat monolayer of carbon atoms tightly packed into a two-dimensional (2D) honeycomb lattice, and is a basic building block for graphitic materials of all other dimensionalities. It can be wrapped up into 0D fullerenes, rolled into 1D nanotubes or stacked into 3D graphite [24]

The last type of allotropes of carbon is represented by the buckminsterfullerenes, or fullerenes, which are a family of spheroidal or cylindrical molecules with all the carbon atoms sp^2 hybridized. In this category are included carbon nanotubes that can be considered as an ordered network of carbon atoms arranged in hexagons to form a seamless hollow cylinder as shown in Figure 2.3.

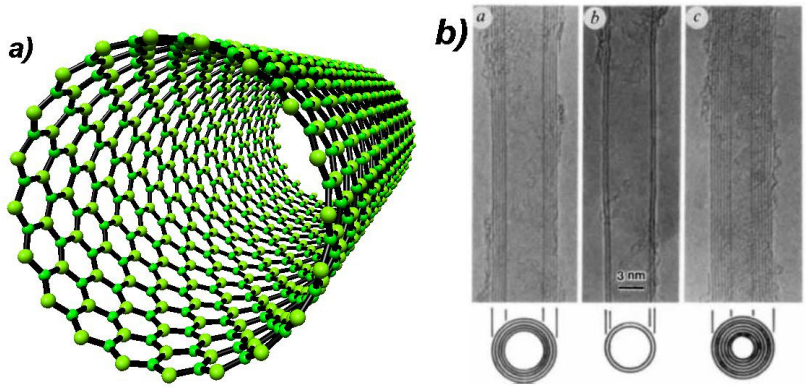

Figure 2.3. a) Carbon Nanotube, b) Carbon Nanotubes as originally reported by Iijima in 1991 [21].

Since their discovery by Iijima in 1991 [21], carbon nanotubes (CNTs) have attracted the interest of researchers because the extraordinary properties. The small diameter (fraction of a nanometre) compared to the extended lenght (up to millimetres), confers to these structures a high aspect ratio identifying CNTs as de facto one-dimensional structures.

Carbon Nanotubes present extraordinary physical and mechanics properties as superior to many other materials commonly used and this fact make CNTs the ideal candidate to replace them in a large number of applications. Ones of the most remarkable properties are the very high tensile strength and Young modulus [30, 31] that makes this material tougher than any other natural or synthetic organic fibre. At the same time carbon nanotubes exhibit high flexibility [25], high termal conductivity [26] and low density [27].

In the field of electrical and electronic properties, carbon nanotubes reveal other incredible features. They can exhibit a metallic behaviour with high conductivity (10^4 S/cm) and high current density (10^6 A/cm^2) [28]. CNTs can also be semiconducting with band gaps ranging from 0 eV to 1 eV [29]. This peculiar behaviour makes them suitable as replacement fo semiconductors in electronic applications, especially when the need of miniaturisation brings the technology to the nanoscale

.

2.1.2 **STRUCTURE OF CARBON NANOTUBES**

Carbon Nanotubes can be further categorized. When the structure considered is an individual cylinder, it is commonly referred to as a single-walled (or single wall) nanotube (SWNT), different from the multi-walled nanotube (MWNT), which is formed when several coaxial cylinders are bonded by van der Waals forces. A third category is identified as double walled nanotube (DWNT) when only two shells form the structure. Single-, Double- and Multi- wall nanotubes are shown in Figure 2.4.

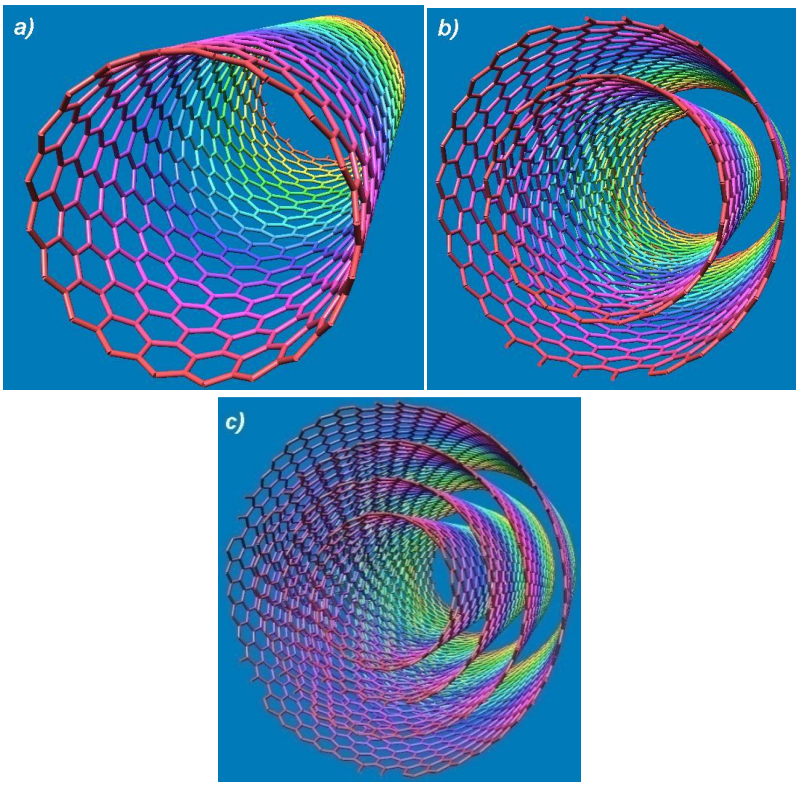

Figure 2.4. a) Single wall carbon nanotube, b) Double wall carbon nanotube. c) Multi wall carbon nanotube.

The way the graphene sheet is rolled determines the fundamental properties of the tube; to describe such a fundamental characteristic of the nanotube we can introduce two vectors, $\mathbf{C_h}$ and **T**, whose rectangle defines the unit cell as shown in Figure 2.5.

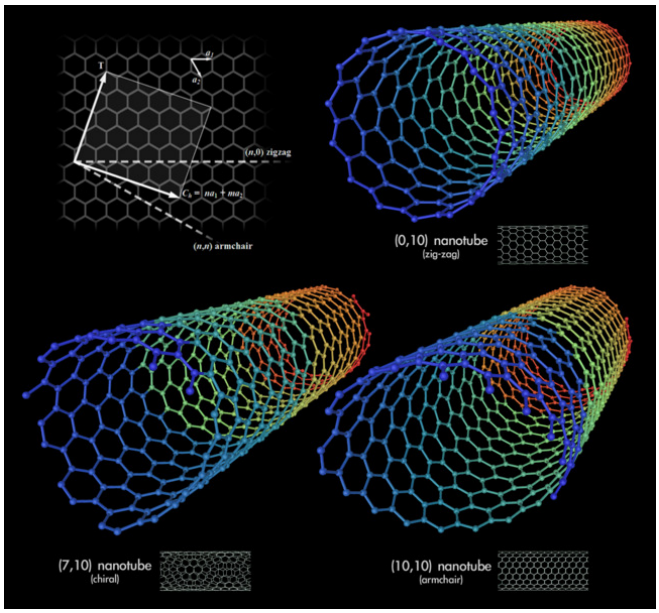

Figure 2.5. The graphene sheet labeled with the integers(n.m). The diameter, chiral angle, and type can be determined by knowing the integers (n,m).

$\mathbf{C_h}$ is the vector that defines that represents the direction of the graphene layes roll and its magnitude is a linear combination of the unit vectors $\mathbf{a_1}$ and $\mathbf{a_2}$ of the hexagonal lattice as reported in the following equation :

$$\boldsymbol{C} = n\boldsymbol{a_1} + m\boldsymbol{a_2} \tag{2.1}$$

The indices (n,m) identify uniquely the nanotube, defining its chirality. Therefore, referring to the reported example, if the layer of graphene is rolled along **C** direction in order to have the coincidence of the (0,0) atom site with the (12,4) one, an infinite lenght (12,4) single wall nanotube has been constructed.

The chiral angle, defined as the angle formed by the chiral vector **C** and the direction of $\mathbf{a_1 + a_2}$, is in the range $0° \leq \varphi \leq 30°$ and is defined by the following equation:

$$\varphi = arcos[\sqrt{3}\,(n+m)/(2\sqrt{n^2+m^2+nm})] \tag{2.2}$$

According to the direction of **C**, and hence to the indices (n,m), three different types of carbon nanotube can be definied, as shown in Figure 2.6. When the indices (n,m) coincide, the structure is an armchair nanotube (φ = 0°); if m=0 the structure is a zigzag nanotube (φ = 30°); in all the other cases it is a chiral nanotube. It is possible to link to each type of carbon nanotube the generating buckminsterfullerene structure, as shown in Figure 2.6. The diameter of the nanotube can be calculated from the indices (n,m) as expressed by the following equation:

$$d = \frac{a}{\pi}\sqrt{n^2 + m^2 + nm} \tag{2.3}$$

where a=0.246 nm is the lattice constant of graphene. The nanotube chirality is an important parameter of the carbon nanotube since, along with the diameter, directly affects the electronic properties of the resultant structure.

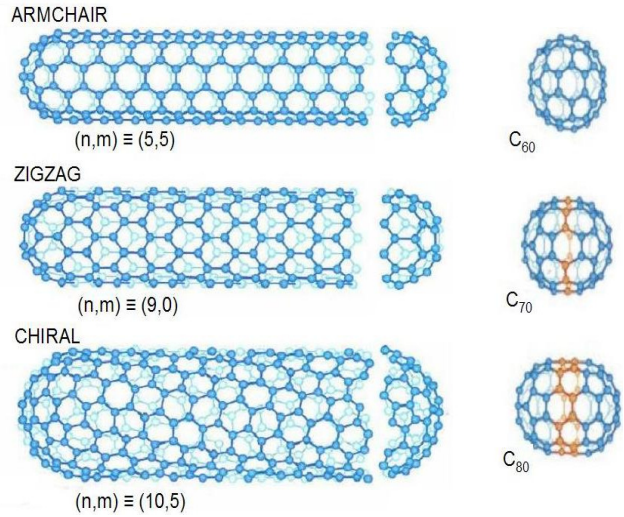

Figure 2.6. Examples of three types of nanotube chirality Armchair, Zigzag and Chiral and the buckminsterfullerene structures from where they can be generated [32].

2.2 SYNTHESIS OF CARBON NANOTUBES

Carbon nanotubes are generally produced by using three main techniques : arc discharge, laser ablation and chemical vapour deposition. In arc-discharge technique, two carbon electrodes are placed at approximately 1 mm distance in controlled inert atmosphere (helium, argon) and, through a controlled power supply, a direct current of 50 to 120 A is driven [22]. The high temperature discharge (3000-4000°C) vapories one of the electrodes and on the other one a rod like deposit is formed. The deposit usually contains soot, fullerenes and MWNTs. The use of transition-metallic catalysts can bring to the growth of SWNTs [33]. High volume production (grams) of SWNTs can be obtained by laser ablation technique. In this method a target of cobalt/nickel and graphite is placed into a quartz tube furnace at 1200°C with an inert atmosphere helium and argon at a pressur of 500Torr. The target is vaporised with a pulsed laser and the hot vapour plume formed expand and cools rapidly. Nanometre-size metal catalyst particles are formed in the plume and assist the growth of SWNTs. At the cold finger terminal inside the furnace, SWNTs assembles in clusters by interaction via van der Waals forces. The yields can vary from 20% to 80% of the weight that also contains graphite, fullerenes, catalysts, etc.

However, the equipment requirements and the large amount of energy consumed by these techniques make them less favorable for CNTs production than Chemical Vapor Deposition (CVD).

For this reason, at the present time, CVD has been identified as the most promising CNTs synthesizing method, as it offers the best prospects for large volume, high purity production of CNTs on different substrates. This method provides a higher degree of control over the morphology and structure of the CNTs produced via the choice of catalyst particle size and various growth conditions. It is achieved by inserting carbon in gas phase (methane, carbon monoxide or acetylene) into a furnace containing a heated up substrate covered with a catalyst (nickel, iron or cobalt). What happens is that a wafer is exposed to these volatile precursors and under determinate conditions they react and decompose onto the substrate to achieve the desired result. Basically, an energy source (plasma or resistively heated coil) transfers energy to the gaseous carbon molecules to “break” them in reactive carbon atoms that diffuse to the substrate and reach the metallic catalyst where they bind. Tipically, CVD temperature ranges from 600°C to 900°C and yields to a 30% CNTs content. Parametres involved in this synthesis process also can range: pressure, gases flow,

temperatures, catalyst, etc.) bringing different properties of the resulting carbon nanotubes.

The following Figure 2.7 shows a schematic of a CVD furnace.

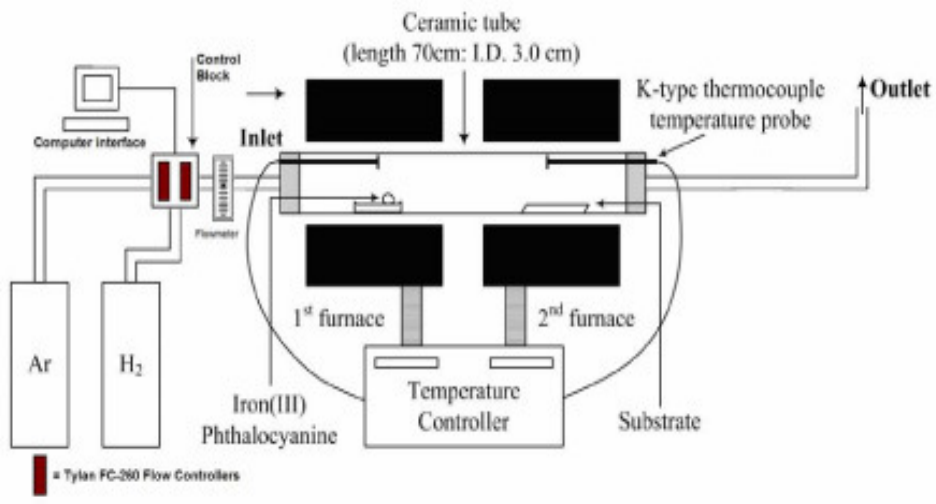

Figure 2.7. Schematic of a two zone atmospheric pressure quartz tube CVD furnace[22].

2.2.1 CVD GROWTH METHOD SPECIFICS

Carbon Nanotubes growth in CVD could be divided into two basic methodologies depending on the location of the catalyst, so called gas phase growth, and substrate growth. Both of them could be split thus there are two different growth pathways : bulk carbon diffusion and surface carbon diffusion models. What happens in gas phase growth is that literally the catalyst formation and nanotube growth occur literally in mid-air. On the other hand, in substrate growth catalyst nanoparticles or metal precursors are deposited either on a substrate such as SiO_2 or on a high-surface area powder before growth.

Both the methods can be classed into surface carbon diffusion and bulk carbon diffusion:

- Surface carbon diffusion : The metal particle continues to be a solid, the cracked carbon diffuses around the surface and on the same side of the metal particle carbon nanotube nucleates. Since carbon continually breaks down on the particle, the tube continues to grow.

This is a common mechanism used to explain low-temperature growth, notably with Ni catalyst nanoparticles. [22].

- Bulk carbon diffusion: The carbon feedstock is cracked on the surface of the metal particle, similar to above. The CNT with one or more walls (SW or MW) starts growning from the outer surface when the nanoparticle dissolving the carbon reaches the saturation.

Both method have been indirectly observed via high-resolution transmission electron microscopy (HRTEM), where the specific favored mechanism by a particular growth method depends on the temperature, the type of metal catalyst, and the carbon feedstock used.

In substrate growth, after the nanotube begins to grow, the CNT will undergo either base growth to tip growth, as illustrated in Figure 2.8. In base growth the catalyst particle remains attached to the surface and the nanotube is extruded into the air or along the surface. During tip growth, the end of the nanotube remains stuck to the surface and the catalyst particle shoots into the air at the opposite end of the extruding nanotube. The two mechanism above mentioned have been used to explain the growth of carbon fibers, MWCNT and SWCNT, relating to the various parameters such as catalyst type, hydrocarbon source and growth temperature. While in SWCNT base growth is considered dominant process, in MWCNT the dominant mechanism is the tip growth

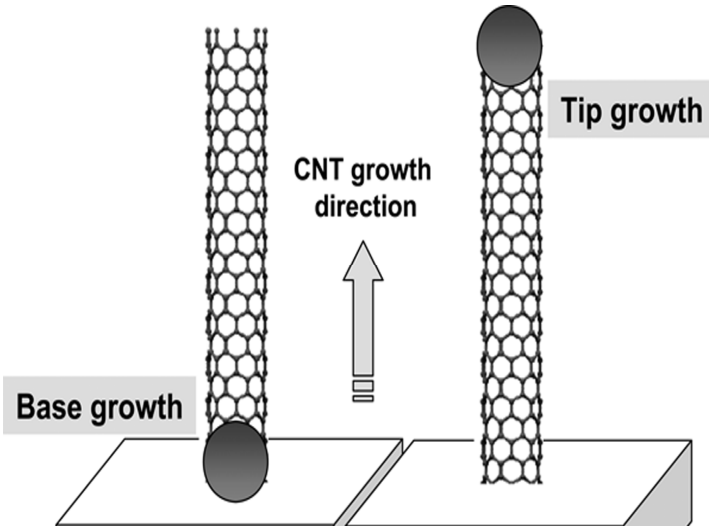

Figure 2.8. Schematic of both tip growth and base growth of nanotube on a substrate [22].

2.2.2 **CARBON FEEDSTOCK**

The first SWCNT synthesis performed with CVD utilized carbon monoxide (CO) as a feedstock. Starting from the first synthesis methane, ethylene, acetylene, ethanol and methanol have been succesfully used in order to achieve always better results to make SWCNT at various temperatures and usign several catalytic metals. There is to declare that there's not a favourite feedstock that could provide clear advantage over the others, though there are many particular applications in which one or another feedstock excel. However an obvious variation in feedstock is reactivity. For example, CH_4 is much less reactive than ethylene (C_2H_4) or acetylene (C_2H_2). As a result, SWCNTs have been grown from C_2H_4 at temperatures as low as 550°C, whereas CH_4 synthesis is not reported below 680°C. Additionally, the oxygen content of the feedstock may have an effect on growth quality and yield. This presence of a controlled amount of oxygen may have a cleansing effect by preventing the formation of amorphous carbon.

2.2.3 **CATALYSTS**

A wide variety of catalytic species can be used in order to obtain SWCNTs or MWCNTs in CVD growth. The word catalyst is used somewhat indiscriminately in nanotube science, wheter or not the catalyst will present its original form after making the nanotube. In CVD growth the most used catalyst are Ni and Fe, and in many cases actually from metal carbides when they produces nanotubes and still mantein them carbides after the process. Regardless to this observation, it has been proved that Fe, Ni and also Co nanoparticles are all able to form SWCNTs. The selection of a metallic catalyst may affect the growth and morphology of the CNTs. For many years, catalyst composition has been limited to iron-group metals above mentioned (Fe, Co, Ni). In the majority of works, well aligned carpets of CNTs have been growth through using these materials, which have the catalytic function of producing graphite on bulk crystal surface. Recently, it has been shown that metallic nano-particleso of many other metals, heavy late-transition (Pd,Pt) and inert metals (Cu, Ag, Au) are also able to act as catalyst in the CVD growth process. However, these materials show different physical and chemical properties. In majority of the works, Fe catalyst had been identified as the best catalyst for CNTs growth by CVD synthesis method.

2.3 CONDUCTING POLYMERS

2.3.1 OVERVIEW

Since their discovery, conducting polymers have attracted the interest of scientists for their potential application in electronics [34,35]. The main structural characteristic of conducting polymers, referred also as synthetic metals, is the π-conjugated system that extends along a number fo recurrent monomers that form the polymer backbone as depicted in Figure 2.9 [36]. This feature derives directly from the sp^2 hybridization of the carbon atoms, in which one *p* orbital remains unperturbed while the other two orbitals and the *s* one combine to form 3 sp^2 orbitals oriented at 120° from each other, as shown in Figure 2.10. Along the direction of the sp^2 orbitals, the σ-bonds constitute the backbone of the polymer while the remaining *p* orbitals form the π-conjugated system that allows electrons to be transported along hte polymer chain direction with reported electrical conductivities up to 10^5 S/cm [37]. The most studied polymers are the following: poly(acetylenes), poly(pyrroles), poly(thiophenes), poly(anilines), poly(p-phenylenes) and poly(paraphenylene-vinylenes). Their easy processability and the possibility of tuning the electrical and optical properties for the specific application make conductive polymers ideal for electronic applications.

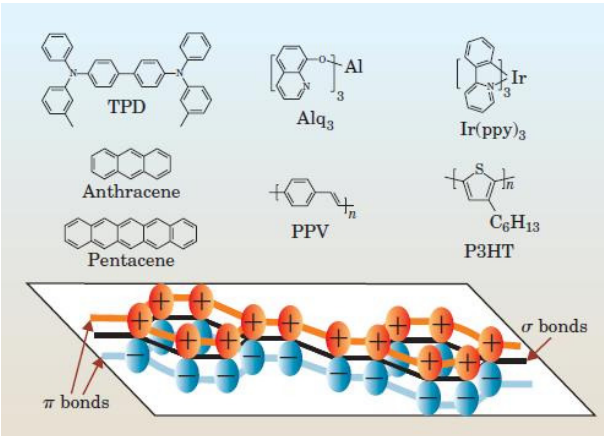

Figure 2.9. Conducting polymer structures [38].

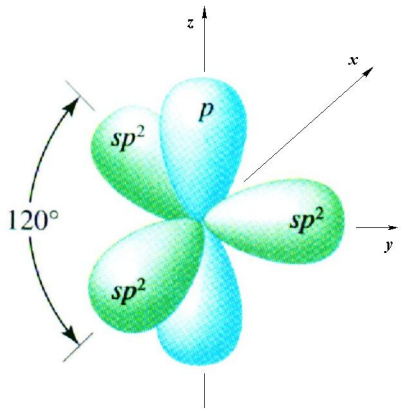

Figure 2.10. sp2 hybridization of the Carbon atom [38].

2.3.2 ELECTRONIC STRUCTURE OF CONDUCTING POLYMERS

All the macroscopic properties of a system can be deduced by knowing the system's wavefunction. Nevertheless, it is common practice to introduce several approximations with various degree of mathematical complexity to model the system and estimate the properties of molecular aggregates. In conducting polymers, the degenerancy of the energy levels is due to the coupling between neighbouring bonding and anti-bonding orbitals in the molecule. This leads to the creation of molecular orbitals (MO). When polymer chains are considered, the interactions between molecular orbitals form quasi continuos bands. The resulting energy bands are separated by energy states not allowed for electrons: the band at lower energy, originating from the bonding orbitals (π), is fully occupied by electrons and is referred as the Highest Occupied Molecular Orbital (HOMO). Conversely, the higher energy band, originating from the anti-bonding orbitals (π*), is empty of electrons and is referred to as the Lowest Unoccupied Molecular Orbital (LUMO). As a matter of fact, bonding and anti-bonding σ orbitals form energy bands too, but the energy separation between π orbitals is smaller (because the overlap is weaker) and so consequently it has a predominant effect on the resulting electronic properties. When a system possesses alternating single and double bonds and *p* interacting orbitals, it is referred as a π-conjugated system and the energy band diagram is similar to the

one reported in Figure 2.11(a) and 2.11(b). At room temperature, according to Fermi distribution function of electrons in energy states and as a result of thermodynamic equilibrium, a few electrons are energetically favoured to occupy part of the energy states in the LUMO and leave empty part of the HOMO band (that can be assumed to be occupied by holes). As a result, electric current can flow through the conducting polymer and, as introduced in the previous paragraph, the π-conjugated system can exhibit a good electric conductivity with high charge mobilities.

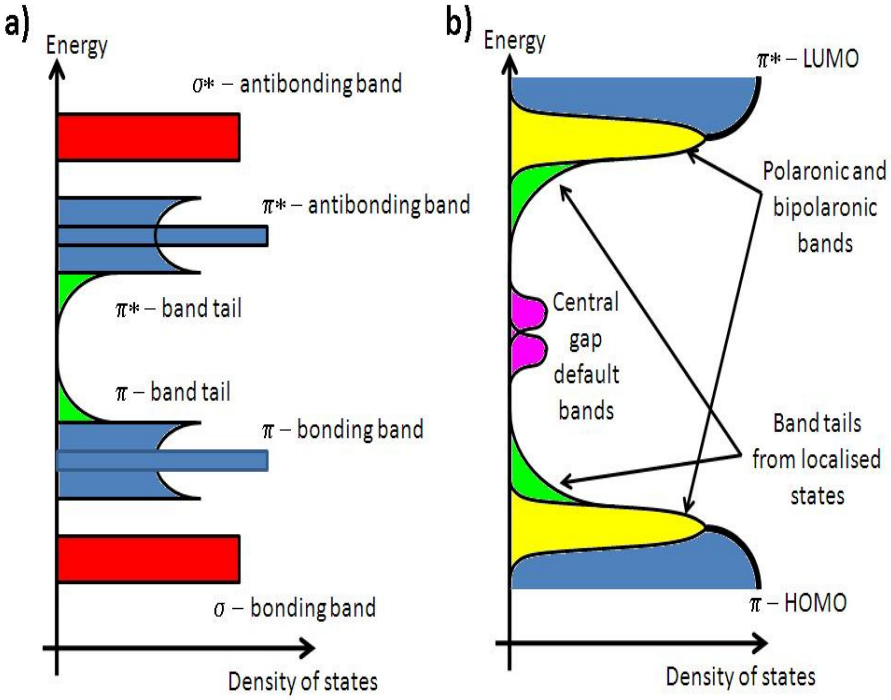

Figure 2.11. Energy bands in π-conjugated polymers [39].

2.3.3 **"REAL ORGANIC SOLID"**

The band diagram of figure 2.11(a) takes into account intra- and inter-chain interactions and distorsions. The overall effect is the presence of energy band tails of allowed states in the forbidden region betweem the HOMO and the LUMO levels that removes the abrupt discontinuity of energy level expected for

isolated polymer chains. As depicted in Figure 2.3(b), allowed energy states and small bands can be present in the case of charge carrier-chain interactions and defects of the polymer chains. These can be structural defects for example during the chemical synthesis or caused by an excess of charge. In this latter case, extra charges localised on the polymer chains can be result of phenomena like: photo excitation, chemical doping (charge transfer from a donor or acceptor type atom or molecule) and charge injection. Since the electronic structure of the π-conjugated system is altered by the presence of defects, these profundly affect the electric and optical properties of the conducting polymer. Referring to single polymer chains, the conjugation lenght represents the number of recurrent monomers with no alteration of the π-conjugated system due to a structural defect. The longer is the conjugation lenght, the higher is the grade of crystallinity and purity of the resultant polymer that approximates an ideal π-conjugated system.

2.3.4 **EXCITONS**

An excitation of an electron from the lowest unoccupied molecular level (LUMO) to the highest occupied molecular level (HOMO) can create a quasi particle referred as "exciton" that corresponds to electron-hole pair interacting through Coulombic forces. In simple terms, the exciton can be regarded as an electron and a hole generated by the absorption of a photon that attract mutually and therefore interact in the same physical space. Depending on the type of solid considered, the exciton can extend in one/few molecules (Frenkel exciton) or several molecules (Mott-Wannier exciton). Mott-Wannier excitons are characteristic of large permitted energy band semiconductors (or large dielectric constants), with electrons and holes that exhibit high mobilities. They can be easily separated since the radius of the exciton is large and the interacting forces are weak. Conversely, Frenkel excitons are characteristic of insulator materials, with low mobilities and low dielectric constants that confer to the quasi-particle a small radius and strong interaction forces. The lifetime of Frenkel excitons is normally short (few nanoseconds) and the diffusion lenght is limited to few tens of nanometres [*]. Excitons are represented as energy states close to the HOMO and LUMO bands as reported in Figure 2.12(a). After the interaction with a photon of energy $h\nu$, the exciton is created as in Figure 2.12(b), but the charges are still interacting and the transport inside the HOMO and the LUMO is not possible. If the separation is completed, the charge carriers reach the respective

energy bands and create/contribute to the current flow as reported in Figure 2.12(b).

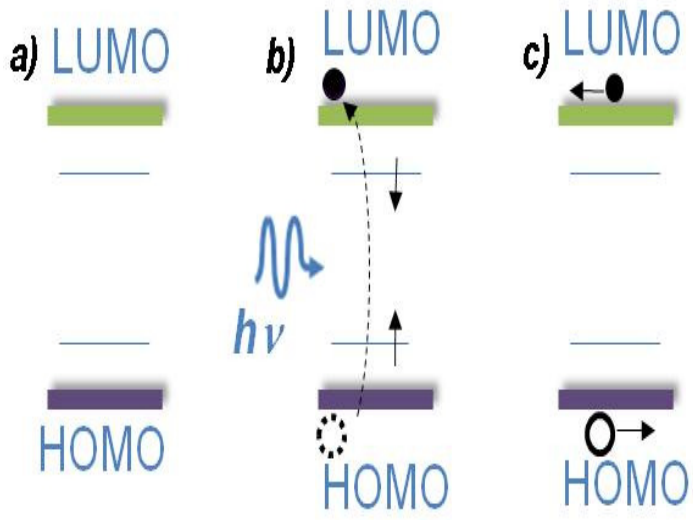

Figure 2.12. a) Exciton states reported with respect to the HOMO and LUMO energy levels, b) Exciton formation after interaction with a photon, c) Free charge carriers transported inside the energy bands.

Exhibiting small dimensions and strong bonds, Frenkel exctions can move through the molecular lattice over hundreds fo molecules by transferring energy to neighbourhood sites. The mechanism of energy tranfer can be through dipolar interactions (long transfer – Forster) or by the overlapping of orbitals (short-tranfer – Dexter). Figure 2.13(a) shows Forster and Dexter tranfer mechanism from an excited donor (D*) to another molecule acting as acceptor (A*). The tranfer occurs only between singlet states and can be written in the form $^1D^*+A \rightarrow {}^1D+{}^1A^*$. Forster mechanism is characterised by the conservation of spin of the single molecules involved and is based on dipole-dipole interactions that are not negligible up to 10 nm (long tranfer). Conversely, in the Dexter tranfer, only the total spin of the system (D*A or DA*) is conserved and does not rely and allowed transitions. Therefore, as depicted in Figure 2.13(a) the same transfer of energy betweem singlet states can occurr leading to the same

final state observed for Forster mechanism. Moreover, as reported in Figure 2.13(b), the Dexter mechanism can allow energy tranfer between the donor triplet to the acceptor following the equation $^3D^*+^1A \rightarrow ^1D+^3A^*$. In this case, the spin is conserved by the system, but is changed for single molecules. The probability of Dexter transfer is related to the surface overlap between molecular orbitals of donor and acceptor molecules. Therefore, it is a short range transfer (up to 2 nm) and decays exponentially with distance.

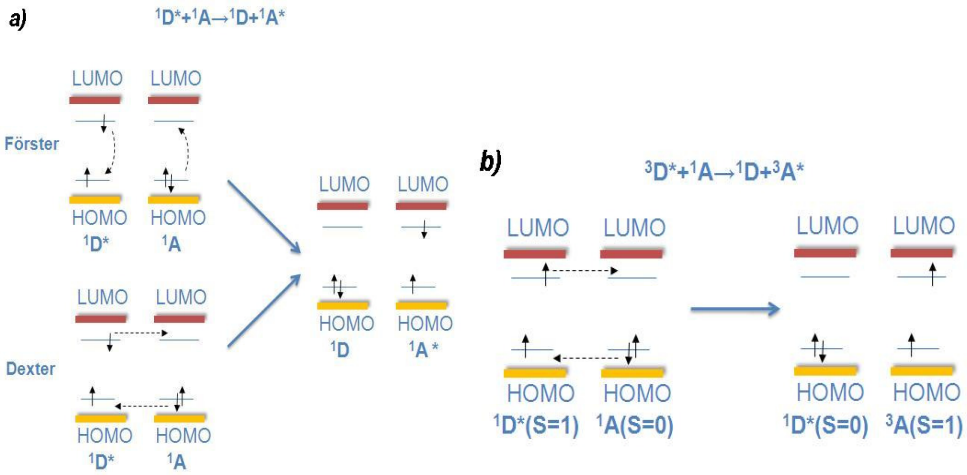

Figure 2.13. a) Exciton transfer between singlet states following Forster mechanism or Dexter mechanism, b) Exciton transfer betweem singlet and triplet states following Dexter mechanism (S=0 denotes a single state, S=1 denotes a triplet state).

3 ORGANIC PHOTOVOLTAICS (OPVs)

3.1 INTRODUCTION

The discovery of electronic conduction in polymers and the synthesis of a conductive polymer demonstrated the possibility of employing new organic materials in electronic applications. Conductive polymers or organic semiconductors rapidly conquered several field of electronic application, being employed since 1990s as active materials for Light Emitting Diodes (LED) and transistors.

Some of the advantages offered by organic semiconductors for potential use in electronics are listed in the following:

- Reduced costs : they can be quite cheap if produced on large scale and their technology costs could be very low considering that the most of the steps used to build a device employ solution processing techniques.
- Improved mechanical and electric properties if compared with inorganic semiconductors like lightness, flexibility, lower power consumption, etc.
- "Tunability" : here intended as the possibility to "tune", by chemical synthesis, the optical and electronic properties of the materials involved in order to adapt them to the requested application.

An example of this technology is represented by the Organic LED display, nowadays a fully recognisable product used in consumer electronics.

The advantages of conductive polymers electronics could have a deep impact on photovoltaic devices. Beyond the previously cited benefits, organic photovoltaics could have the following attractive potential features:

- to be manufactured with printing processes and continuously;

- to be semitransparent (window coating);

- to produce directly in large area devices;

- to allow easy device integration

- to be economically and environmentally advantageous.

The potential low cost of organic photovoltaics can be compared with silicon solar cell production by using a simple calculation. If the typical 30 cm silicon wafer annual production in terms of area is assumed 88000 m^2/year, considering a sheet feed offset printing (1-3 m/s) for OPVs, the same production could be achieved in 10 hours [40]. The following figure 3.1 is a schematic representation about the difference between an inorganic solar cell and an organic solar cell.

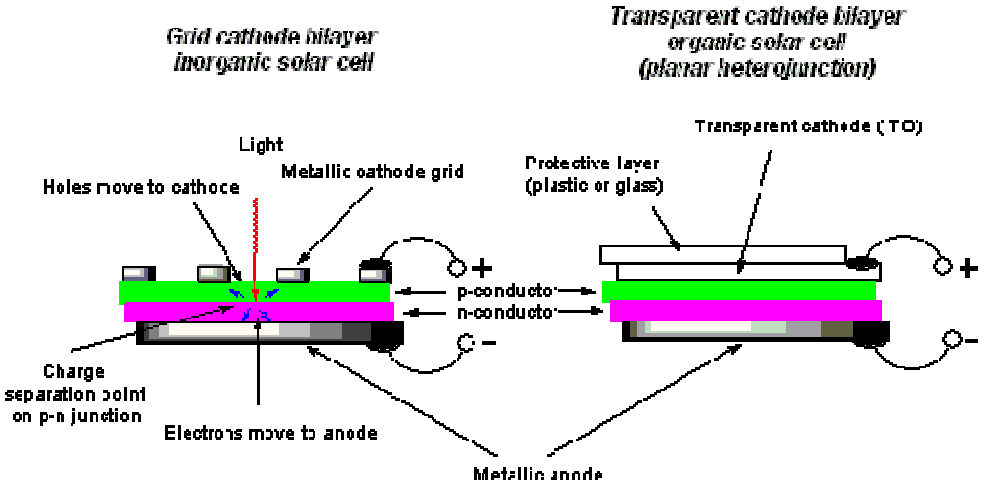

Figure 3.1. Difference between inorganic solar cell and organic solar cell [41].

3.2 **BULK HETEROJUNCTION SOLAR CELLS**

Although photovoltaic effects in a conjugated polymer were observed in 1981, many problems didn't allow the use of this technology limiting the direct employment of these materials for photovoltaic applications. At first, the photon absorption does not generate free charge carriers since the charges of the electron-hole pair created are bound toghether in an exciton. Due to the high binding energy required to completely separate the charges, a large proportion of the photogenerated exciton charges recombine and thermally decay. The second major difficulty affects the separated charges that have to be transported through the medium. Since the conductivity of conjugated polymers is not high, the devices show a significant series resistance that lowers the overall perfomance. Moreover, many conjugated polymers are hole-conductive, with mobilities higher than the electrons's by several orders of magnitude. Therefore, effective bipolar transport can be enormously reduced with dramatic consequences on the power conversion efficiencies.

To overcome both difficulties, the doping of polymers with high electron transport materials has been proposed. The polymer is supposed to act as donor of electrons (D) while the dopant is considered the acceptor of charges (A). If the materials employed show a significant energy difference between electron affinities, the electric field arising at the separating interface increases the probability of charge separation. First attempts were made by stacking two layers of different polymers [42] or blending two polymers network [43], recording an increase of charges collected of several orders of magnitude. Good results have also been obtained by depositing stacked layers of a donor polymer onto acceptor nanostructures like buckminsterfullerenes [44]. Although the results were promising, the limitation of this approach is that charge separation is obtained only in the space in close proximity to the two media interface, where the interface electric field is located. Considering that excition diffusion lenghts and lifetimes are normally short, the probability of charge separation is strongly affected by the grade of interpenetration of the two networks.

In 1992, Sarifitci [45] introduced the concept of bulk heterojunction solar cells based on the inclusion of nearly-spherical nanostructures (buckminsterfullerenes or simply fullerenes) into the polymer matrix, as depicted in Figure 3.2.

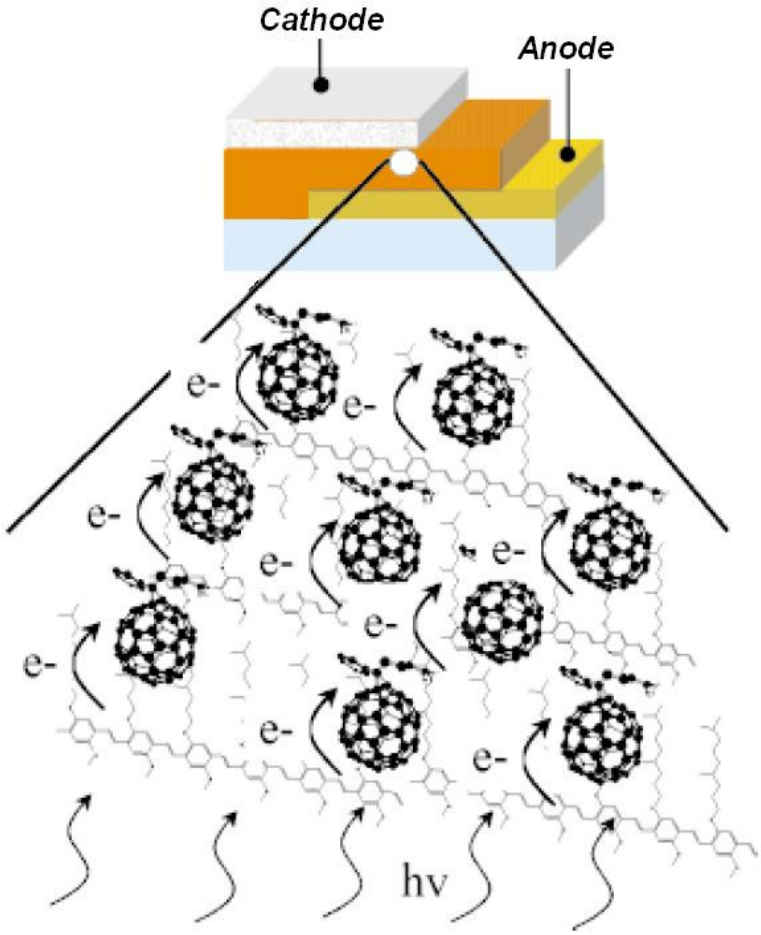

Figure 3.2. Charge creation, separation and transport in bulk heterojunction devices. The nanostructure is represented by spheres while the polymer is the bulk material. After the photon absorption holes are collected on the anode contact and electrons migrate amon [16].

Blending the polymer with nanoscale materials (about 10nm diameter quasi-spheres) yields a heterojunction surface distributed uniformly throughout the device active layer and hence charge separation is favoured. Indeed, the probability of exciton is heavily raised; behind this there's the reason that the

charge separation time can be 10^3 times faster than exciton thermal decay time (ultrafast photocharge separation) [45]. The consequence could result in a improved power conversion efficiency of about two orders of magnitude [46].

3.3 WORKING PRINCIPLE OF BULK HETEROJUNCTION SOLAR CELLS

When the nanostructure is introduced in the polymer matrix, the two materials interact and a bulk heterojunction is formed. Indicating with D the donor unit and with A the acceptor one, under illumination the photoinduced charge transfer can be described with the following processes:

I. $D + A \rightarrow {}^{1,3}D^* + A$ [excitation of donor to a singlet or a triplet state]

II. ${}^{1,3}D^* + A \rightarrow {}^{1,3}(D\text{-}A)^*$ [excitation delocalised on the D-A complex]

III. ${}^{1,3}(D\text{-}A)^* \rightarrow {}^{1,3}(D^{\delta+}\text{-}A^{\delta-})^*$ [charge transfer initiated]

IV. ${}^{1,3}(D^{\delta+}\text{-}A^{\delta-})^* \rightarrow {}^{1,3}(D^{+\cdot}\text{-}A^{-\cdot})$ [ion radical pair formed]

V. ${}^{1,3}(D^{+\cdot}\text{-}A^{-\cdot}) \rightarrow D^{+\cdot} + A^{-\cdot}$ [charge separation]

Extremely fast responses, of the order of picoseconds [45] or femtoseconds [47] have been observed for conjugated polymer interpenetrated with fullerenes, giving charge separation quantum efficiencies close to unity. The migration of electrons to the acceptor phase and the permanence of holes in the donor phase highlight the possibility to ulitize bulk heterojunction blends for photovoltaic applications. In fact, the interpenetration of the two materials places virtually any point in the active media at few nanometers distance to a donor-acceptor interface. Considering the simple energy band materials as depicted in Figure 3.3(a), with χ_{ED} and χ_{EA} have been indicated the electron affinities of the donor and of the acceptor respectively. When the materials are mixed and the blend is formed, it can be assumed that due to the mismatch of the Fermi energy in the two semiconductors, an electrostatic potential is present at interface and plays a fundamental role in the exciton separation favouring the electron migration to the acceptor phase.

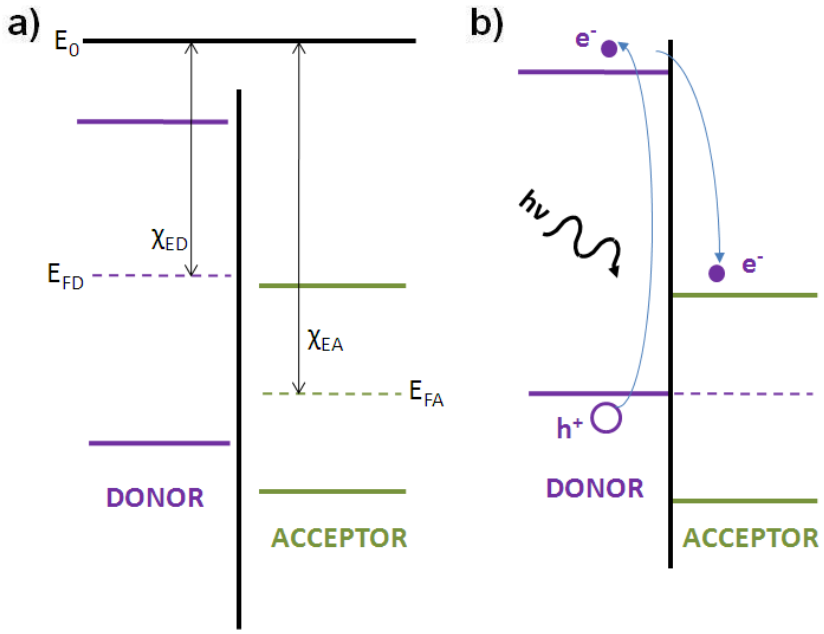

Figure 3.3. a) Isolated materials prior the heterojunction creation. b) Photocharge generation upon light absorption and electron migration.

In order to take into account all mechanisms affecting the photovoltaic generation and the harvesting of charge in bulk heterojunction solar cells, a model based on six processes, numbered form 1 to 6, has been proposed and is reported in Figure 3.4. The photon is absorbed (1) by the organic polymer and generates an exciton (2). The exciton diffuses inside the polymer (3) until it encounters the built-in electric field at the interface of the heterojunction. Here, the separation occurs (4), leaving the hole in the donor material and the electron in the acceptor phase. The two separated charges are transported inside the donor and inside the acceptor (5), in the latter case by multi-hopping through adjacent nanostructures. Once the electrodes have been reached, the carriers are ready to be collected (6).

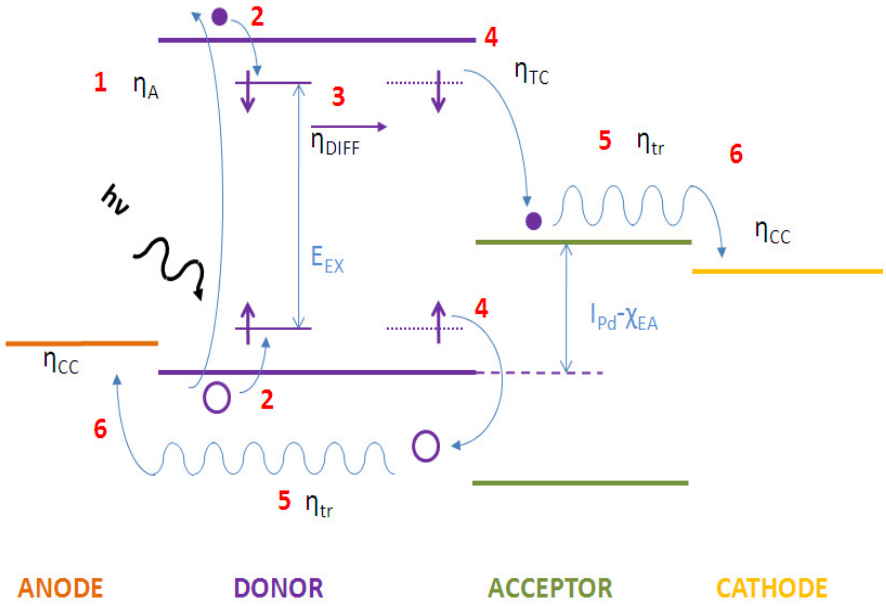

Figure 3.4. Six mechanism involved in the photovoltaic effect in bulk heterojuntion solar cells.

The six mechanism briefly reported in the following. To each mechanism can be associated a characteristic efficiency indicated with η:

1) Photon absorption $\boldsymbol{\eta_A}$ (related to the absorption coefficient material);
2) Exciton creation $\boldsymbol{E_{EX}}$ (characterized by the exciton energy);
3) Exciton diffusion $\boldsymbol{\eta_{DIFF}}$ (lowered by the recombination processes that may occur);
4) Exciton separation $\boldsymbol{\eta_{TC}}$ (affected by the materials involved);
5) Charge transport by diffusion $\boldsymbol{\eta_{tr}}$ (related to charge mobilities in the two phases and affected by defects and impurities);

6) Charge collection η_{CC} (dependent from the position of the Fermi energy levels of cathode and anode contacts);

The exciton separation process is profoundly affected by band aligments of the materials involved. In fact, the exciton binding energy is E_{GAP}-E_{EX} with E_{GAP} the energy gap of the light absorbing material. Although E_{GAP}-E_{EX} can be low (0.1-0.2eV), Peumans [48] have reported the condition for an efficient charge separation, as depicted in Figure 3.5(a) and (b). If IP_D is the ionization potential of the donor and χ_{EA} is the electron affinity of the acceptor, a high probability of exciton separation is achieved for $E_{EX} > IP_D - \chi_{EA}$. If this condition is not matched, the charge separation is less likely to occur and the power conversion efficiency of the solar cell will be lowered. Another condition affecting the performance of the photovoltaic device is the energy position (work function) of anode and cathode contacts. As reported in Figure 3.4, the conditions to be matched are $(E_F)_{cathode} < (E_{LUMO})_{acceptor}$ and $(E_F)_{anode} > (E_{HOMO})_{donor}$. If matched, η_{CC} can be considered close to unity.

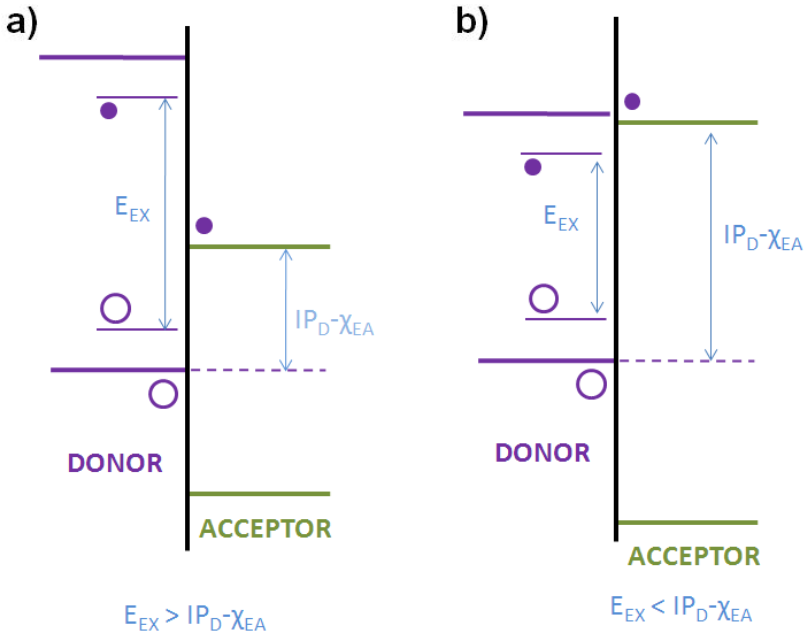

Figure 3.5. a) efficient exciton separation in bulk heterojunction solar cells. b) non-efficient exciton separation in bulk heterojunction

As can be expected, the band alignments of the materials involved in the building of the devices play an important role on the values of the short circuit current, the fill factor and the open circuit voltage. In particular, the origin of open circuit voltage in bulk heterojunction solar cells has been interpreted according to different models and V_{OC} has been individuated as one limiting factor to device performance [49]. The *pn* junction model cannot be used since the typical open circuit voltages observed in the range of 0.5-1 V cannot be related to optical band gaps of polymers and nanostructures (in the range of 2-2.5 eV).

The first interpretation was given by using the simple Metal-Insulator-Metal (MIM) model, that relates the V_{OC} to the energy difference between the anode and cathode electrodes energies [50]. The model needs to be adapted introducing the Fermi level pinning at donor-acceptor interface to take into account the strong influence of reduction potential of fullerenes on the open circuit voltage [51]. Further analysis brought Koster [52] to propose a MIM model that takes into consideration also the effect of open circuit voltage on light intensity and the related energy separation of quasi-Fermi levels. Another approach was followed by Schraber [53] that empirically interpreted several experiment data. A good agreement was found for fullerene based devices by relating the V_{OC} to the difference between the HOMO level of the donor and the LUMO level of acceptor, according the following equation:

$$V_{OC} = \frac{1}{q}\left(\left|E_{HOMO}^{Donor}\right| - \left|E_{LUMO}^{Acceptor}\right|\right) - 0.3V \tag{3.1}$$

where q is the charge of the electron. Although there is a multitude of models found in literature, the interpretation of the device performance and their relation with the materials electronic properties is still controversial.

3.4 MATERIALS FOR OPVs

3.4.1 POLYTHIOPHENES

The thiophene molecule, reported in Figure 3.6, is a hetero-cyclic, aromatic compound characterized by a flat five-membered ring identified by the formula C_4H_4S. Thiophene monomers linked through the positions 2-5 form the

backbone of polythiophene polymers. In general polythiophenes are easier to handle than other conductive polymers because are less sensitive to oxygen. Moreover, the simple preparation of substituted monomers (alkyl groups) brings to better solubility and higher electrical conductivities. Polythiophenes are synthesized with three methods: chemical oxidation, coupling with organometallic agents and electrochemical oxidation.

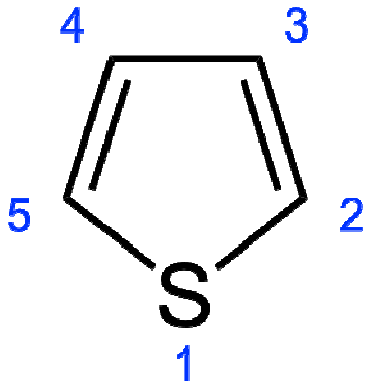

Figure 3.6. Structure of the thiophene monomer.

3.4.1.1 **Poly(3-hexylthiophene) (P3HT)**

Poly(3-hexylthiophene) are commonly used as the conductive polymer in photovoltaic applications owning to its good electrical conductivity properties and good processability. Poly(3-hexylthiophene) can be synthesized into 2 forms, namely regiorandom P3HT (rraP3HT) and regioregular P3HT (rrP3HT) as depicted in Figure 3.7.

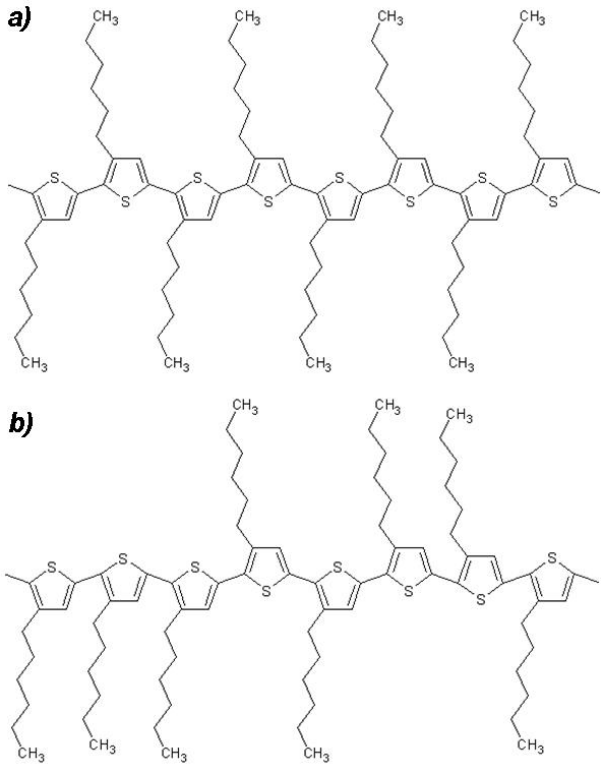

Figure 3.7. Poly(3-hexilthiophene) in the form a) regioregular and b)regiorandom

It can be considered as p-type semiconductors with high hole mobility up to ~0.1$cm^2V^{-1}s^{-1}$[54]. This type of polymer has been the popular choice for the following reasons :

- Regioregular polythiophenes have appreciable level of spatial order that contributes to the high inter-chain carrier mobilities.
- P3HT has high hole mobility under comparison with other types of polymer such as poly(3-ocylthiophene) (P3OT).
- High optical absorption coefficient estimated around $1x10^5cm^{-1}$ in 400-600nm region of the solar spectrum.
- Promising efficient electron conducting path when assemble with SWNTs. In this work, P3HT will be blend with PCBM on different level of concentration to achieve the best photovoltaic layer for the polymer solar cell.

3.4.1.2 **Poly(3,4-ethylenedioxythiophene):Poly(styrenesulfonate) (PEDOT:PSS)**

Pedot is a conjugated polymer that is positively doped and neutralized with PSS polyanion. It is used as an electron blocking layer in organic photovoltaic devices. The structure is reported in Figure 3.8 in its benzoic and quinoid form. Since it offers many advantages when compared to other π-conjugated polymers, such as high transparency, excellent thermal stability and aqueous processability, PEDOT:PSS has been used for many electronic applications.

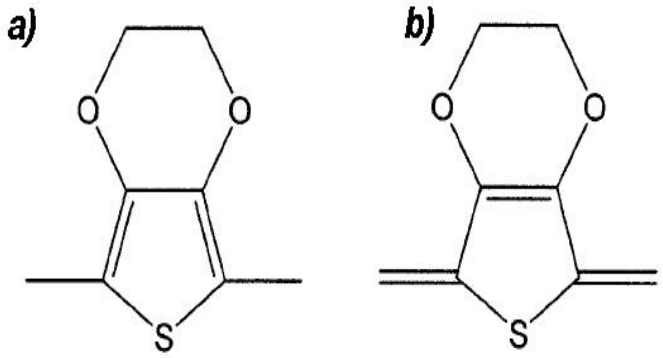

Figure 3.8. PEDOT:PSS structure in its a) benzoic and b) quinoid form.

PEDOT:PSS layer is necessary to adjust SWCNTs work function for hole collection and to avoid the device from shorting by having the metallic nanotubes transport electrons from the PCBM network to the transparent electrode. The polymer photovoltaic cells in this project will be fabricated with and without PEDOT:PSS layer to investigate their behavior.

3.4.2 **FULLERENES**

At present, the best power conversion efficiencies for organic photovoltaic devices have been reached using fullerenes and fullerene derivatives as electron acceptors. Fullerenes are carbon-based molecules formed by several carbon atoms like carbon nanotubes that can be considered as a particular type of fullerene of cylindrical form. One of the most common forms of fullerene is Buckminsterfullerene that consist of 60 or more atoms or of carbon (C_{60}, C_{70}, etc.) as shown in Figure 3.9 (a).

To improve its solubility in organic solvents, it is common to find Buckminsterfullerenes in their functionalized form (PCBM and BM-C60) as depicted in Figure 3.9 (b) and (c). For this project PCBM is the fullerene used as the electron acceptor for the polymeric mixture P3HT-PCBM.

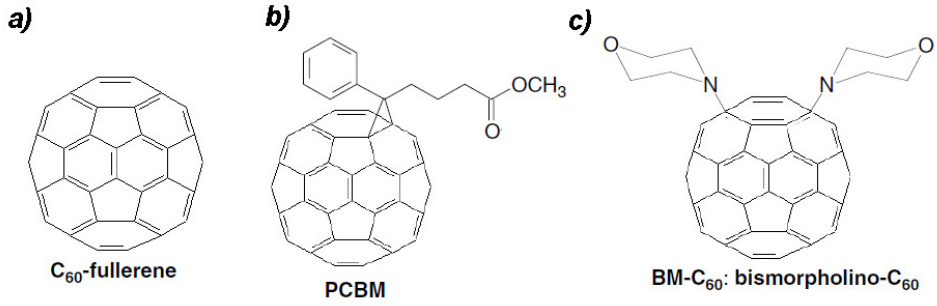

Figure 3.9. Buckminsterfullerenes: C_{60} (a), PCBM (b), BM-C_{60}(c).

4 METHODOLOGY AND FACILITIES

The purpose of this chapter is to describe and illustrate all the facilities and methods that allow the creation and the study of the Organic Solar Cell since the first steps, including the cleaning, until the last step represented by the final characterization of the created sample.

4.1 CNTs GROWTH

The most important step for this project is CNTs growth. They are grown, via Chemical Vapor Deposition (CVD) on an indium tin oxide (ITO) glass substrate. These glass samples with ITO layer offer an electrically conductive surface and high optical transparency that is a perfect match for OPVs devices.

Firstly, before the CNTs growth, the substrate is treated in a cleaning-process, including an ultrasonic cleaning that uses ultrasound (from 20-400 kHz) and water, as shown in Figure 4.1(left):

- Ultrasonic baths in acetone (CH_3-CO-CH_3) for 5 minutes or more;
- Ultrasonic baths in Milli-Q water, that has been purified and deionized to a high degree by a water purification system, for 5 minutes or more;
- Dry the sample with Nitrogen Gas (N_2).

Figure 4.1. The ultrasonic cleaning used for the samples (left) and gas tanks (right).

All this process should ensure a high level quality and purity of the substrate before the important step of the CVD in which the carbon nanotubes are growing.

The CVD process involves a series of parameters and devices that need to be listed:

- Gas choice: Acetylene, Hydrogen, Argon as shown in Figure 4.1(right);
- Gas flow control to mix of the gases (flow measurement term *sccm*), pictured in Figure 4.2(left);
- Furnace made by a ceramic tube and two chambers and the relative temperature/process controller for each chamber, all represented in Figure 4.2(right);
- Fume cupboard for security reason.

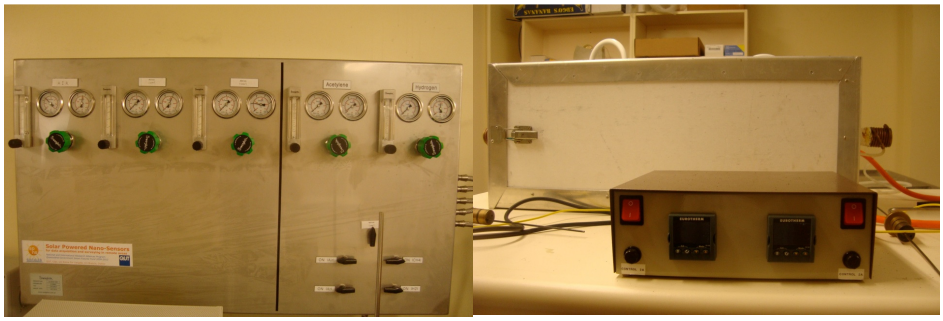

Figure 4.2. Gas flux control (flow measurement sccm) in the QUT laboratory.

As specified in the previous list, the gases involved in the CVD processes are Argon, Hydrogen and Acetylene. Once the sample (glass with ITO) has been washed and inserted in the ceramic tube of the furnace, Argon is used first for cleaning the chamber without initiating any chemical reaction. Indeed the name is derived from the Greek word ***αργον*** meaning "the inactive one" referring to the fact that the element undergoes almost no chemical reaction. The chamber is flushed for 10 minutes prior the second step.

The second gas involved in the process is Hydrogen. It flows with Argon, once the cleaning process is over and the temperature for CNTs growth is set, by Temperature/Process controller, in a range varying from 600 to 500 °C. In this way the process is heading to the heart of the CVD. In fact, when the established temperature is reached, generally after 10-12 minutes, the Argon flow is completely stopped and a mixture of only Hydrogen and Acetylene starts to

enter in the furnace. The CVD process that uses Acetylene and Hydrogen mixture takes 15, 30 or 45 minutes depending on the desired growth of the CNTs. In this way large area high density arrays of CNT carpets are synthesized on both ITO and glass substrate. In the meanwhile the fume cupboard is always on to prevent the presence of harmful fumes in the working environment.

The temperature/process controller is then switched off and in this way the ceramic tube and the furnace are allowed to cool down to room temperature; after almost two hours the sample can be collected and it is possible characterize CNTs with a Scanning Electron Microscope (SEM).

4.2 ORGANIC PHOTOVOLTAIC DEVICE FABRICATION

In this chapter the most important phases for the organic device fabrication are presented. The classic one follows a specific outline; once the Indium Tin Oxide is ready, the electronic blocking layer of PEDOT:PSS is deposited by spin coating, then another blend of polymer/nanotube is deposited always by spin coating. For the final metallic back contact, either aluminium, silver or gold are used; a schematic representation of the device is shown in Figure 4.3.

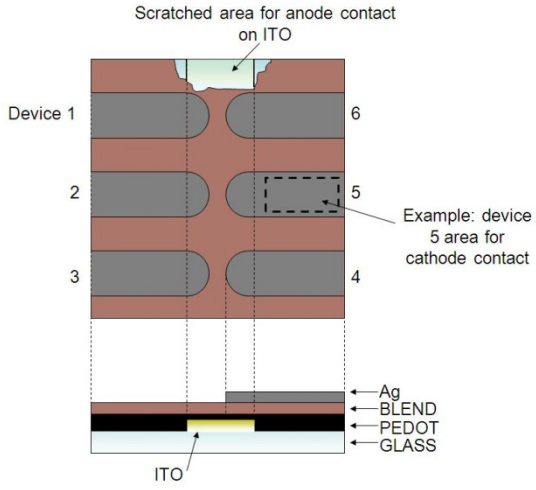

Figure 4.3. Polymer/Nanotube composites device schematic diagram

In this project will be used ITO + Pedot and pure ITO, beyond ITO + CNTs, as transparent electrodes for the final solar cell.

The composite deposition can be done by drop casting or by spin casting. The first is used for characterisation of the bulk properties of the film and when there is no need of controlled morphology of the film. Conversely, by spin casting the composite solution, a controlled and reproducible thickness of the layer can be achieved and therefore this technique is frequently used to deposit the stacked layers of the solar cell. In this project spin-coating is the established way for the composite deposition. Figure 4.4 shows the spin-coating process.

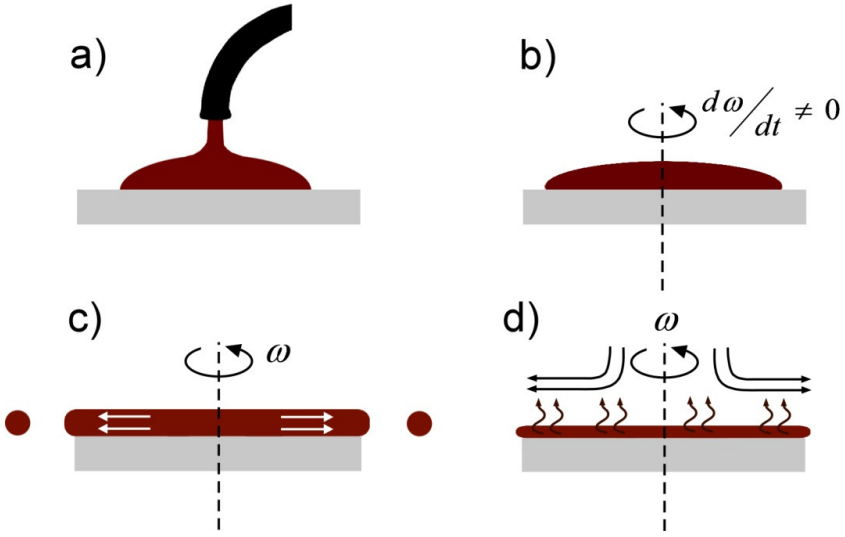

Figure 4.4. Spin-Coating scheme (S. L. Hellstrom, Stanford University 2007).

The polymer and the nanotube solutions can be mixed in two main ways: by stirring or sonication. Stirring is largely used for polymer and fullerenes solution mixing [***]. It is normally carried out for several hours at moderate temperatures (40-50 °C). Conversely, when nanotubes are used, the mixing with the polymer solution is made principally by sonication or with combination of stirring and sonication [**].

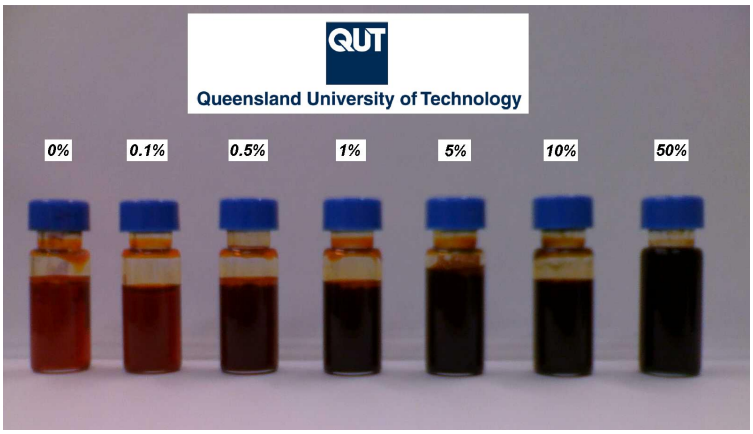

Figure 4.5. Example of various polymer/CNTs composites dispersed in chloroform. The numbers shown represent the relative weight content of the CNTs load.

The metal electrode fabrication is obtained by thermal evaporation. This technique consists By resistively heating the aluminum to its evaporation temperature, a thin layer is deposited on the target substrate. In order to achieve a clean and uniform layer without the formation of oxides, the chamber is kept at a pressure of 10^{-4}-10^{-6} Torr (High Vacuum).

Figure 4.6 illustrates the thermal evaporation process and Figure 4.7(left) shows the metal evaporator E6500 MHVE Bench Top Evaporator.

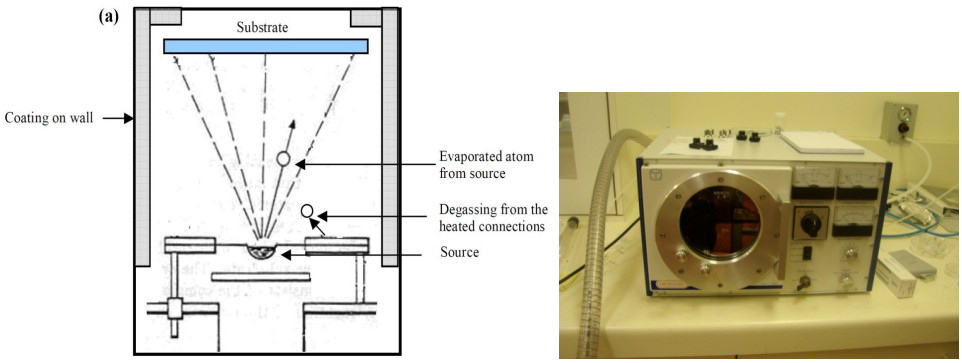

Figure 4.6. Scheme of the thermal evaporation (left) and E6500 MHVE Bench Top Evaporator (right).

All the processes are carried out in a Glove Box ; Figure 4.7 shows an image of this technology.

Figure 4.7 Glove Box.

4.3 MICROSCOPY and ANALYTICAL FACILITIES

4.3.1 SCANNING ELECTRON MICROSCOPE (SEM)

In all the experiments performed by the CVD furnace, surface of substrates are imaged with a highly-sophisticated FEI Quanta 200 3D Scanning Electron Microscope (SEM) before and after the growth; preliminary analysis on the chemical composition of the result after CVD process are conducted by Energy Dispersive X-Ray (EDX). SEM is one of the most widely used techniques in characterisation of nanomaterials and nanostructures. It provides results that allow a better understanding on the structure and behaviour of the growth; so appropriate adjustment can applied on the parameters and procedures to improve the next CNTs growth.

Resolution of the SEM approaches a few nanometers with adjustable magnifications ranging from ~10 to over 300000. Other then providing the morphology and microstructure of bulk and nanostructured materials or device, SEM also provides the detailed information of the chemical composition near the surface.

In typical SEM, as shown in Figure 4.8 and Figure 4.9, a source of electrons is focused into a high energy beam (ranging from few hundred to 50 keV) having very precise pointing size of ~5nm. These electrons are projected in a raster manner over the surface of the sample. The emitted electrons are collected through a cathode ray tube (CRT) that produces the SEM images for

characterisation. Given numerous types of SEM images produced through various SEM techniques and parameters, the principle images produced in SEM can generally be classified into three categories; namely the secondary electron images, backscattered electron images and elemental X-ray maps.

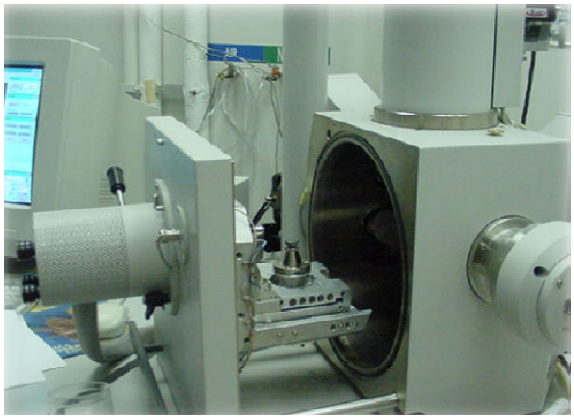

Figure 4.8. Scanning Electron Microscope opening the sample chamber.

With the combination of the high resolution and chemical analytical capabilities of SEM techniques, no doubt it is the most widely implemented techniques for characterisation of the photovoltaic devices.

Figure 4.9. Scanning Electron Microscope (SEM) system.

5 EXPERIMENTAL RESULTS

This chapter is a report of all the experiments that have been running during the time in QUT. To obtain a comparison of the final solar cells efficiency, different values of the parameters involved in the growth of CNTs via CVD have been utilized (catalyst, highest CVD temperature, time CVD deposition).

Three different electrodes, ITO+PEDOT, ITO only and ITO+CNTs have been tested to investigate the V_{OC}, I_{SC}, FF and Efficiency.

5.1 CNTs GROWTH AND CHARACTERIZATION

In this paragraph we present the CVD synthesis carried out on ITO coated glass covered by a thin layer of Fe or Ni catalyst Firstly, in order to define the best CNTs synthesis parameters, many experiments have been conducted using different Acetylene and Hydrogen flows with different selection of CVD parameters (temperature, flow rate, etc). Figure 5.1 shows a schematic representation of the position of the substrates in the porcelain boat.

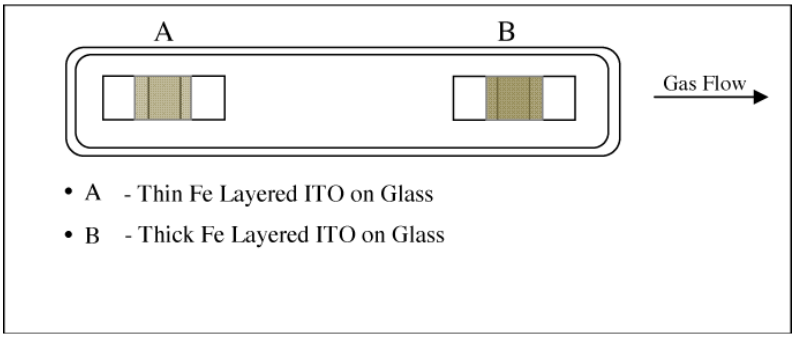

Figure 5.1. Position of the substrate in the porcelain boat.

Before the CVD growth, the ITO substrates are cleaned by the procedures described in the previous chapter; after cleaning, a film of iron catalyst with the desired thickness is coated onto the ITO substrates using the E6500 MHVE Bench Top Evaporator; Figure 5.2 (a) shows the difference between thin Fe coated ITO (A) and thick Fe coated ITO on glass substrate (B). The 5nm Ni deposition has been done in UQ (University of Queensland) by sputtering (Figure 5.2 (b)). The CVD process takes place in the atmospheric pressure ceramic tube CVD furnace. Four trials are performed with temperatures ranging

from 550°C to 600°C and with different gas ratio between Argon (120sccm and 100sccm) and Acetylene flow rates (30sccm, 15sccm, 20sccm) respectively. The substrates are placed in a specific spot in the porcelain boat positioned inside the tube, where temperature is measured by the controller.

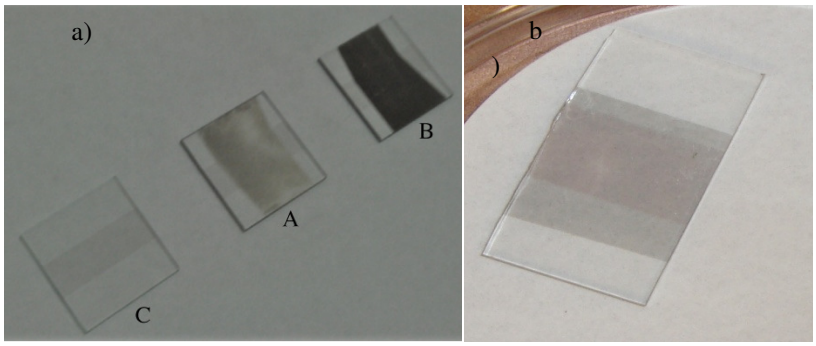

Figure 5.2. a) From the left side: pure ITO on glass substrate (C), thin Fe coated ITO on glass substrate (A), thick Fe coated ITO on glass substrate(B). b) Ni ITO on glass substrate.

For the thin layered Fe coated ITO and the thick layered Fe coated ITO on glass substrates, called ITO A and ITO B, the procedure is as follows. The CVD chamber is initially purged under 200sccm of Argon flow for 5 mins. Thereafter, the Argon is regulated to the desired flow rate and the temperature is increased at a rate of 20°C/min until it has reached the desired temperature proposed for each trial. At the desired deposition temperature, Acetylene is allowed to flow for a period of time, until it is reaching the proposed growth time for each trial. A conformal thin film of iron catalyst on ITO with good adhesion to CNT arrays is generated via iron-catalyzed pyrolytic decomposition of Acetylene. The furnace is then switched off and allowed to cool down to room temperature, under 200sccm of argon flow. The optimized process condition, selected from the characterization of the CNT film morphologies and correlating the results based on the various experimental growth conditions, are listed in Table 5.1

For the ultrathin Fe coated ITO on glass substrate, called ITO 1, ITO 2, ITO 3, a list of the most important parameters for the metal evaporation is presented in Table 5.2. In these experiments the initial flow of Argon is 1000sccm for 5 minutes for ITO 2 and always the same rate, 1000sccm, but for 10 minutes for ITO 1 and ITO 3. After that Argon and Hydrogen are push to the desired flow rates and the temperature is increased at 20°C/min to the desired temperature; once this temperature is reached, the Argon flow is stopped and a flow of Hydrogen and Acetylene is charged for the CVD growth. The furnace is then

switched off and it is cooled down by a 100sccm flow of Argon. The different parameters are reported in Table 5.1.

Table 5.1. Main results of the experimental runs using different catalyst and different CVD parameters (ordered by decreasing temperature).

ITO name	Catalyst	CVD Flow Rate	T (°C)	Growth Time (min.)	Results
ITO A	Fe: 10nm	Argon:120sccm Acetylene:30sccm	600 °C	10	Good yield of thin layer of CNTs
ITO B	Fe: 20nm	Argon:120sccm Acetylene:30sccm	600 °C	10	Good yield of thick layer of CNTs
ITO C	Fe: 10nm	Argon:100sccm Acetylene:10sccm	550 °C	15	Good yield of thin layer of CNTs
ITO D	Fe: 20nm	Argon:100sccm Acetylene:10sccm	550 °C	15	Good yield of thick layer of CNTs
ITO E	Fe: 10nm	Argon:100sccm Acetylene:10sccm	550 °C	25	Deteriorated thin layer of CNTs
ITO F	Fe: 20nm	Argon:100sccm Acetylene:10sccm	550 °C	25	Deteriorated thin layer of CNTs
ITO G	Fe:10nm	Argon:100sccm Acetylene:15sccm	550 °C	30	Best yield of thick layer of CNTs
ITO H	Fe: 20nm	Argon:100sccm Acetylene:15sccm	550 °C	30	Best yield of thick layer of CNTs
ITO 4	Fe:10nm	Argon:200sccm Acetylene:30sccm Hydrogen:30sccm	550 °C	30	High yield of thick layer of CNTs
ITO 3	Fe:3nm	Hydrogen:150sccm Argon:15sccm	550 °C	30	High density distribution of CNTs
ITO 7	Ni:5nm	Hydrogen:150sccm Argon:15sccm	525 °C	15	After CVD substrate too dark. No SEM analysis
ITO 2	Fe:3nm	Hydrogen:150sccm Acetylene:15sccm	520 °C	30	High density distribution of CNTs
ITO 6	Ni:5nm	Hydrogen:150sccm Acetylene:15sccm	500 °C	15	No traces of CNTs
ITO 5	Ni:5nm	Hydrogen:150sccm Acetylene:15sccm	500 °C	30	Compact block distribution of CNTs
ITO 1	Fe:3nm	Hydrogen:150sccm Acetylene:15sccm	500 °C	30	Good density distribution of CNTs

Table 5.2. Metal Evaporation parameters for ITO 2 and ITO 1.

Metal Evaporated	Deposition Pressure (mbar)	Cleaning with shutter Time (s)	Metal Evaporation Time (s)	Current Intensity (A)
Fe	1.7×10^{-4}	31.83	42.20	20

For the Ni coated ITO on glass substrates, named ITO 4, ITO 5, ITO 6, ITO 7 the process is almost the same used for ITO 1 and ITO 3. The difference is in the cooling process; in these samples a 1000sccm Argon flow is passed for 5 minutes (for all of them) immediately after the CVD growth process. After which a 100sccm Argon flow is passing for 30 (ITO 4 and ITO 6) or for 60 minutes (ITO 5 and ITO 7).

In Table 5.3 Resistance values are presented for ITO 1, ITO 2, ITO 5 and ITO 6 before and after the CVD.

Table 5.3. Resistance values for ITO 1, ITO 2, ITO 5 and ITO 6

ITO name	Resistance before CVD (Ω)	Resistance after CVD (Ω)
ITO 1	50 Ω	300 Ω
ITO 2	50 Ω	115 kΩ
ITO 5	50 Ω	15 kΩ
ITO 6	50 Ω	14 kΩ

It is very important to know resistance values in order to select the appropriate ITO substrate for the proposed solar cell. The first observation that can be made is that the resistance values increase significantly; the degradation of the electrical conductivity of the substrate is due to the chemical reduction of indium and tin oxides to their corresponding metallic elements [55]. Comparing the resistance values for the different substrate, ITO 1 presents the best behaviour about the rising temperature due to the CVD process, showing a resistance value of 300Ω after the CNTs growth; however, before selecting ITO

1 as the ideal electrode for the proposed solar cell, it is appropriate to investigate all CNT film structures by Scanning Electron Microscope (SEM).

Upon the completion of the CVD growth, a black carbon layer appeared on the surface of the substrates coated with an Iron or Nickel catalyst. Figure 5.4 contains the SEM and EDX analysis of the sample grown . The SEM micrographs suggest that the black compound on the ITO substrate is a carpet of of CNTs, as confirmed by EDX analysis.

From the SEM micrographs it is possible to obtain the first indications about the effect of different experimental parameters on the CVD growth process. At first it is possible to observe that the rate of CNT growth on ITO much slower than on glass substrates. This is probably due to the contamination of the Ni and Fe catalysts from Indium (In) in the underlying ITO. ITO glass is known to contaminate the active layers in organic light emitting diodes with these materials, neither of which are known to catalyse CNT growth. This reduced growth rate is advantageous in the present context since it enables a very high degree of control over CNT height required for utility in organic solar cell (<200nm). The CNTs grown on the glass surface demonstrates the possibility of synthesizing CNTs directly on glass substrate when a higher degree of control in synthesizing process is developed. The following Figure 5.3(a) and (b) show the different growth rate on both ITO and glass on ITO G substrate.

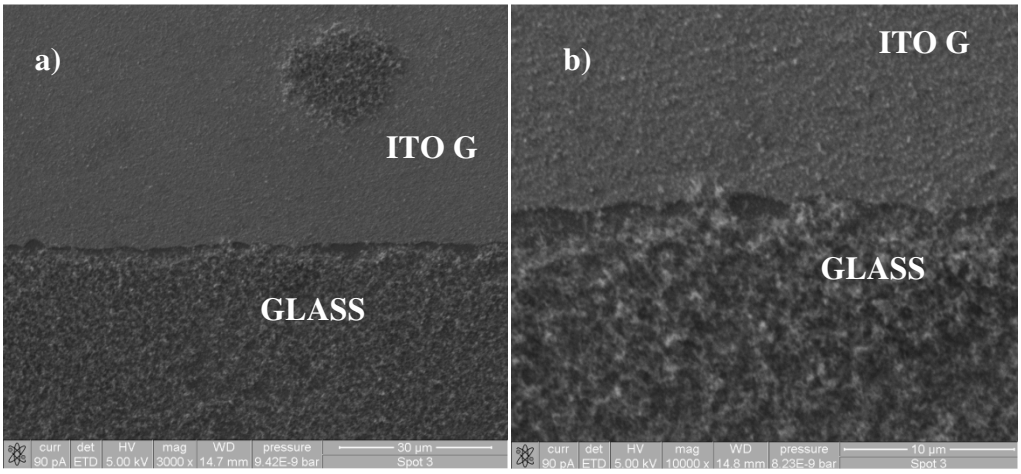

Figure 5.3. a-b) SEM images of CNTs film on ITO G and glass surface showing the difference between the different growth rate on glass and on ITO.

Comparing the results obtained from ITO B (Figure 5.4), grown at 600°C, and ITO D, (Figure 5.5) grown at 550°C, the CNT carpets are found to have

different thickness. The carpet synthesized in sample ITO D is more suitable for the proposed organic solar cell, as it is made of shorter nanotubes, which can provide conduction without short-circuiting the device. Nevertheless we decided to use a range of 100°C centred around 550°C to have a better understanding of the temperature influence on the growth.

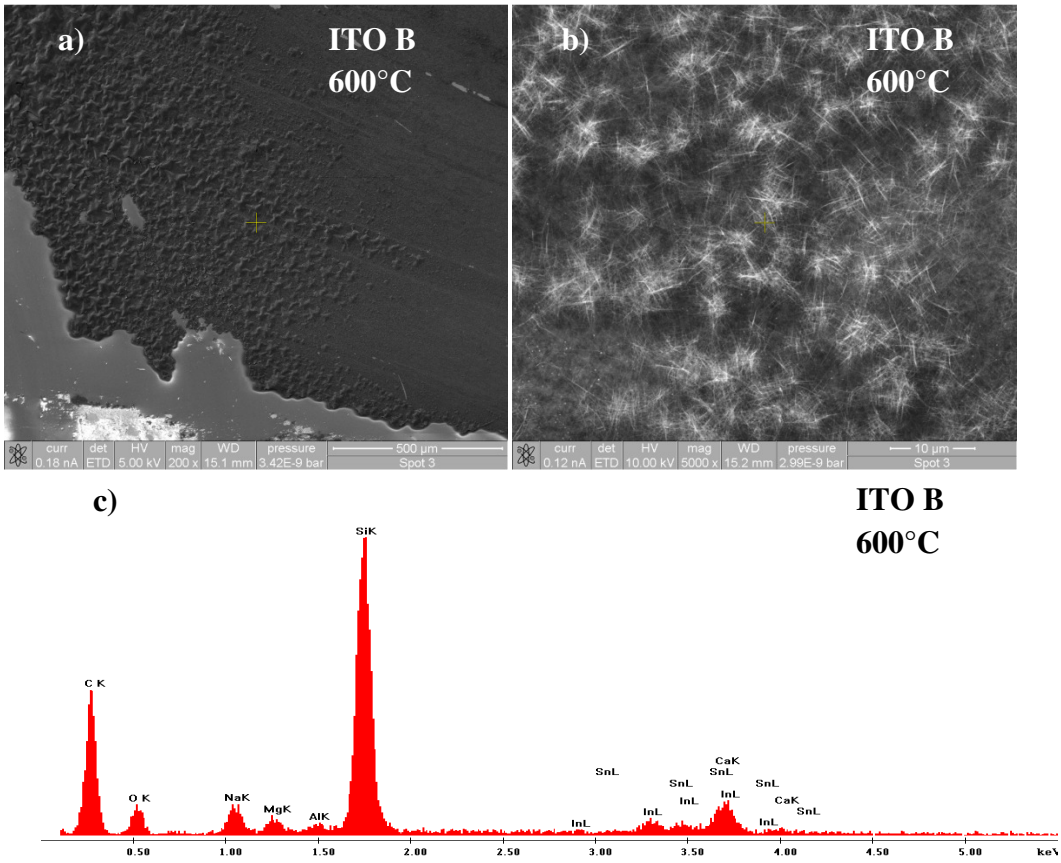

Figure 5.4. a-b) SEM images of CNTs film on ITO B surface synthesized with Argon flux of 120sccm and Acetylene flux at 30sccm. CNTs growth time 10 minutes at 600°C. c) EDX analysis of the substrate.

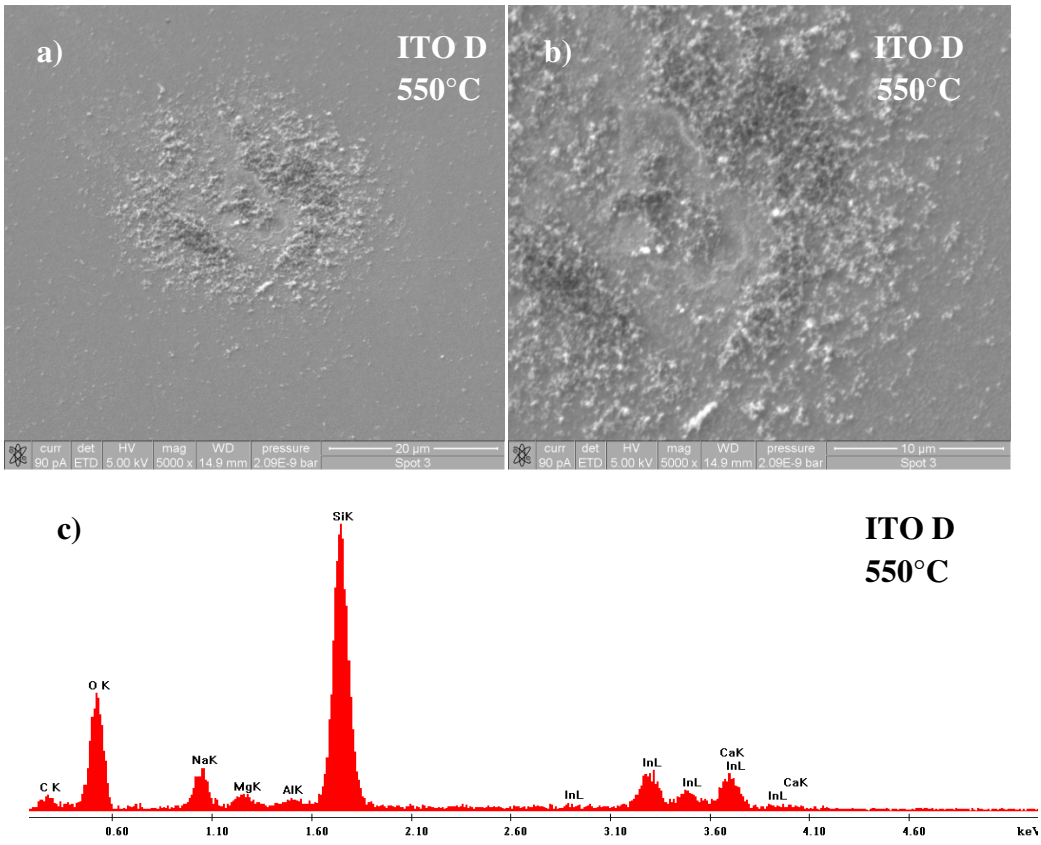

Figure 5.5. a-b) SEM images of CNTs film on ITO D surface synthesized with Argon flux of 100sccm and Acetylene flux at 10sccm. CNTs growth time 15 minutes at 550°C. c) EDX analysis of the substrate.

The catalyst is another important parameter to be controlled in our experiments; in fact CNTs growth is very sensitive to the thickness of the deposited Fe (or Ni) catalyst. This effect can be seen qualitatively in the SEM images for CNTs synthesized on ITO C, shown in Figure 5.6, and ITO D, represented in Figure 5.5; in ITO C the 10nm Fe deposition reduces the thickness of the CNT carpet

Comparing the results for ITO C (10nm Fe deposition) with the previous ITO D it is possible to see that the CNT film presents a more uniform distribution and a lower density; thus ITO C is more suitable than ITO D for the proposed solar cell.

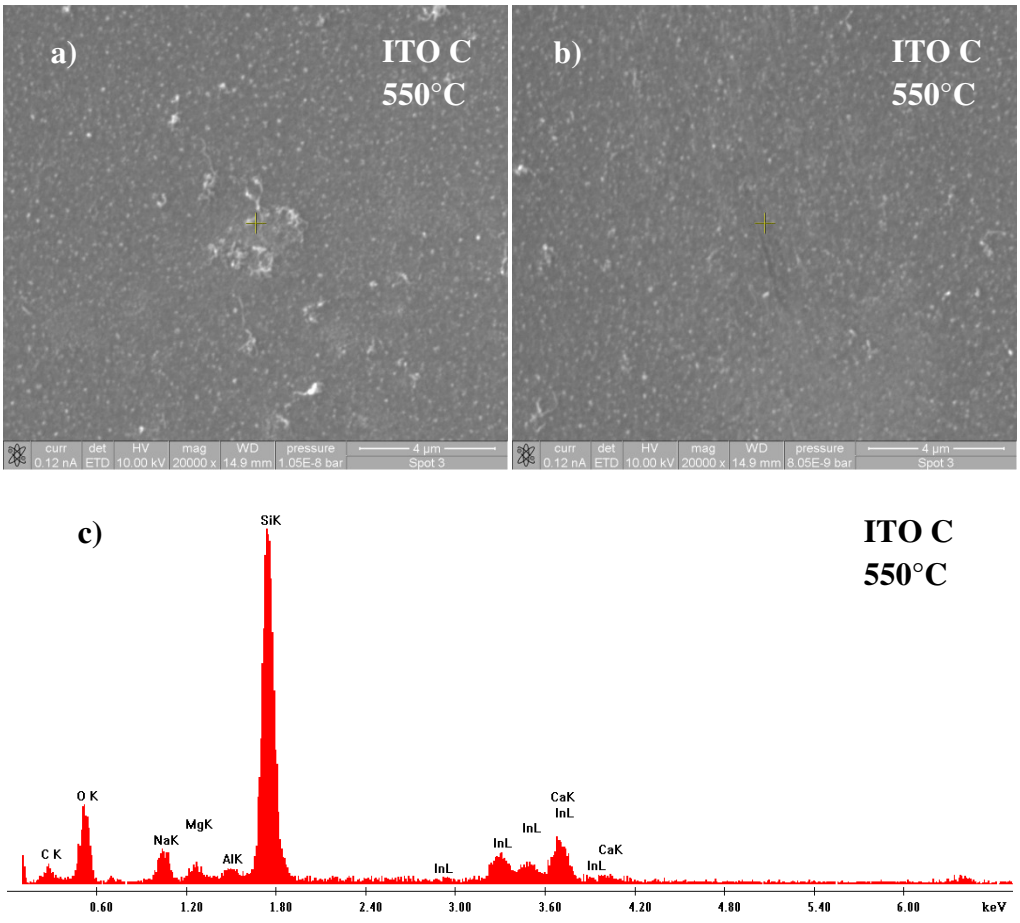

Figure 5.6. a-b) SEM images of CNTs film on ITO C surface synthesized with Argon flux of 100sccm and Acetylene flux at 10sccm. CNTs growth time is 15 minutes at 550°C. c) EDX analysis of the substrate.

ITO E and ITO F present deteriorated CNT layers; this could have been caused by contamination of the substrate or by inaccuracies in the control of the gas flow.

For the next substrates it is introduced a change of flowing gases to understand how they affect the behaviour of the CNTs growth. For ITO 4 there are three gases involved in the CVD process: Argon, Hydrogen and Acetylene. The experiments start from 550°C decreasing to 500°C. For ITO 1, 2 and 3 the gases used for the CVD process include Hydrogen and Acetylene, with the same flow rate.

The SEM image for ITO 4, obtained using Argon and Hydrogen, shows a reduced density in the CNT carpet compared to ITO G, obtained using Acetylene. The difference between the two substrates is due to the flow gases used for the CVD process. This reduction in CNT density gives us a further indication about the rightness in change the gases used for the CVD process; in fact CNT density is one of the key parameter for the desired CNT growth. For this reason from this experiment the gases used for the CVD will be Hydrogen and Acetylene.

Figure 5.7 shows the difference between the ITO G and ITO 4:

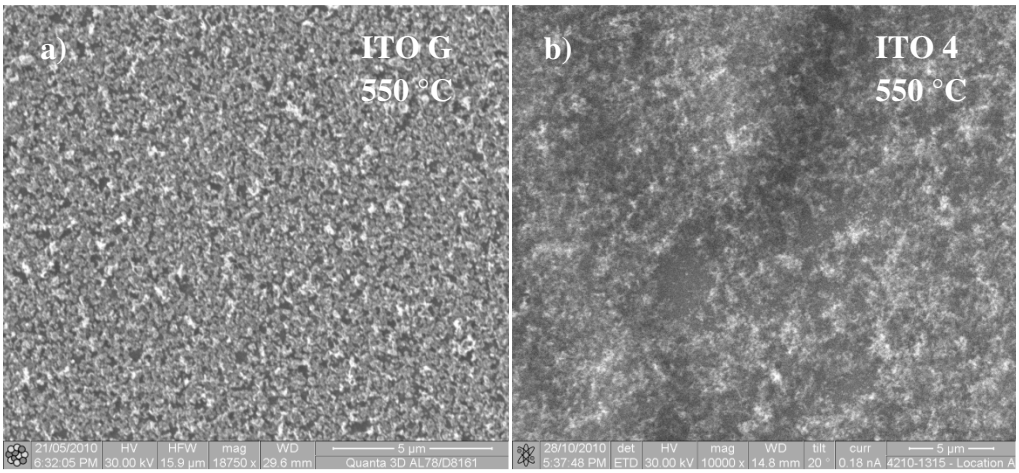

Figure 5.7. a) SEM image for the CNTs carpet in ITO G substrate. b) SEM image for CNTs carpet in ITO 4 substrate.

As said before, reduction in deposited catalyst thickness on the surface of the ITO (and on the glass substrate) is another important indication given by SEM images about the substrates obtained from the experiments. For this reason the Fe thickness is reduced to 3nm for ITO 1, ITO 2 and ITO 3. The following SEM images refer to the ITO substrates that have 3nm Fe deposition. In order to find the best parameters for the CNTs growth, temperature and CNTs growth time are changed. A 15sccm Acetylene flux and an 150sccm Hydrogen flux are used to synthesize the nanotubes on the substrate surface. Figure 5.8 shows the SEM image for the synthesis results for ITO 3 while Figure 5.9 (a) and (b) shows the CNTs carpet in ITO 2.

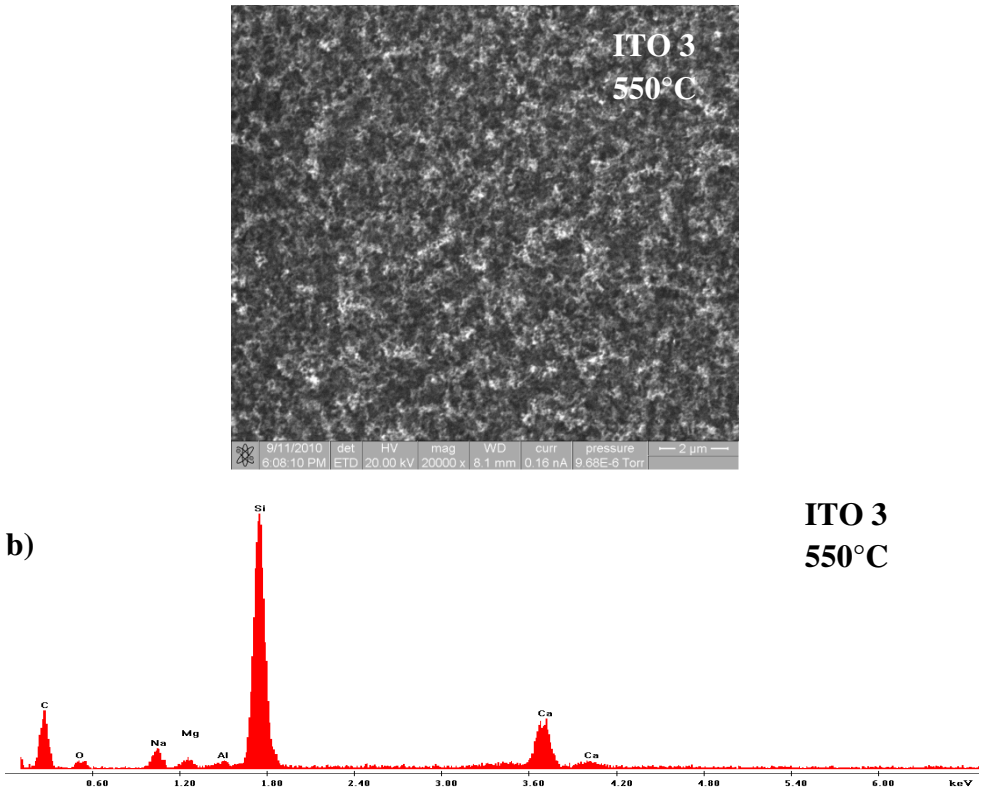

Figure 5.8. a) SEM image of the CNTs film on ITO 3 surface synthesized with Acetylene flux of 15sccm and Hydrogen flux at 150sccm. CNTs growth time 30 minutes at 550°C. b) EDX analysis of the substrate.

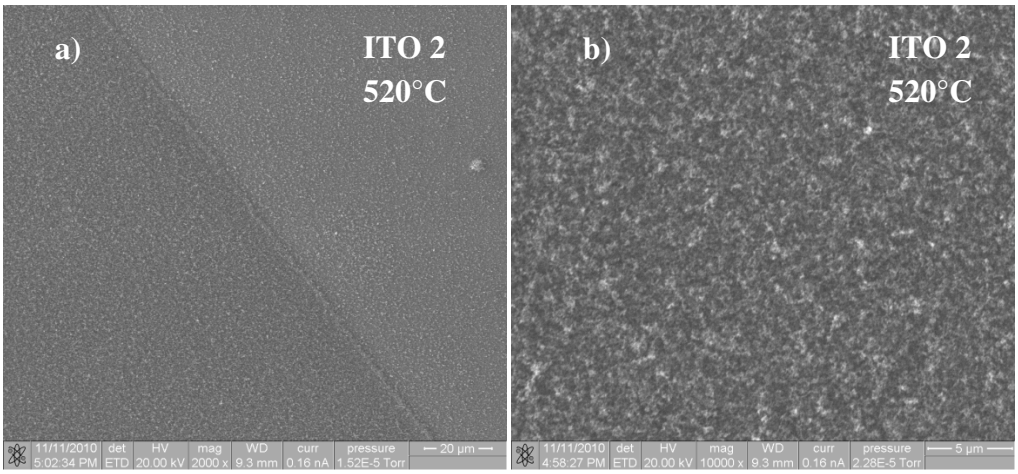

Figure 5.9. a-b) SEM image of the CNTs film on ITO 2 surface synthesized with Acetylene flux of 15sccm and Hydrogen flux at 150sccm. CNTs growth time 30 minutes at 520°C.

Figure 5.9 (b) shows a more uniform coverage of nanotubes compared to ITO 3, but unfortunately it is not transparent, making impossible the utilization for organic photovoltaic application.

In Figure 5.10 we present the results of the CVD process using 5 nm Ni catalyst (ITO 5) instead of Fe. We suppose that a minimum Ni layer thickness of approximately of 5 nm is required for the growth due to the rapid diffusion of Ni into the polycrystalline ITO during CVD.

Observing Figure 5.10 a very high density CNTs carpet can be seen at first; analysing more the image it is possible to notice an high CNTs height (>500nm) and this is not a suitable feature for using the ITO + CNTs as the transparent electrode in the solar cell. This is due to the high height CNTs measure, about 1μm, in contrast for the request of <200nm CNTs to avoid problems associated with electrical shorting. In Figure 5.11 is reported an ITO 5 photography immediately after the CNTs growth, showing the black compound onto the surface of the substrate.

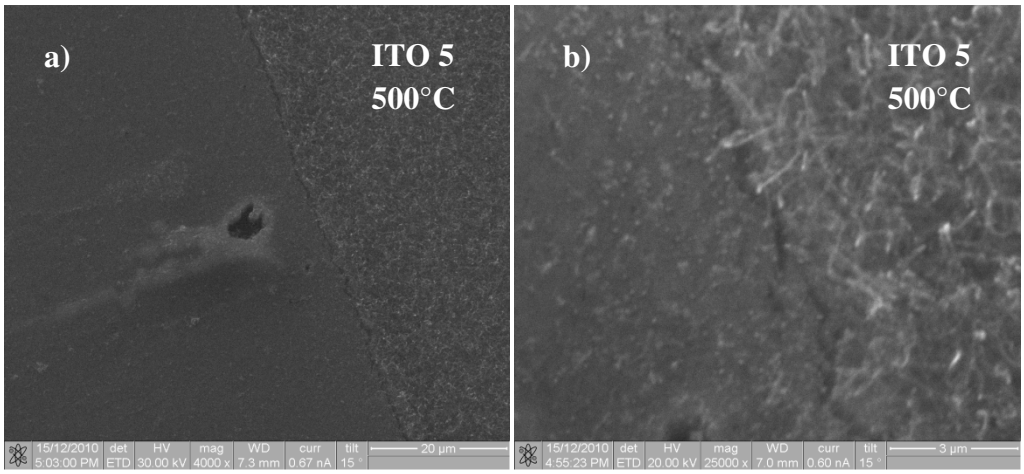

Figure 5.10. a-b) SEM images of CNTs film on ITO 5 surface synthesized with Argon flux of 120sccm and Acetylene flux at 15sccm. CNTs growth time 30 minutes at 500 °C.

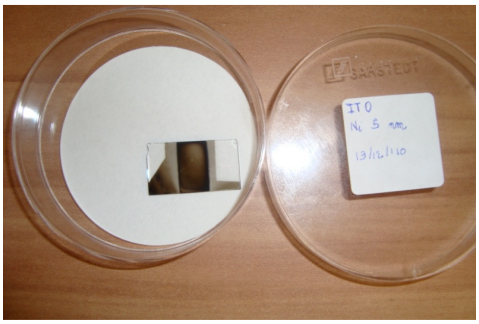

Figure 5.11. ITO 5 photography after the CNTs growth.

As ITO 5 is not suitable due to the height of the CNTs obtained and for a too high resistance value, we still need to search for another sample.

ITO 1 presents the most suitable features to be used as the transparent electrode for the solar cell. The following parameters have been used in order to obtain the CNTs carpet on ITO 1; 3nm Fe as catalyst, 150sccm of Hydrogen and 15sccm of Acetylene, 500 °C as growth temperature and 30 minutes for the growth time. In ITO 1 the synthesized CNTs have, on a quality level, heights in the order of 200nm; this is a desirable property for the proposed organic solar cell. CNTs in this range of height present different key advantages that can be a better the mechanical stability of the contact by directly bond CNTs to the ITO substrate, ensure that all CNTs are in direct contact with the underlying ITO

electrode to ensure a continuous pathway to the external circuit and, finally, CNTs height of <200nm is sufficiently short to allow the CNTs penetrating into the P3HT:PCBM layer without extending all the way to the counter-electrode.

The SEM images for ITO 1 are presented in Figure 5.12.

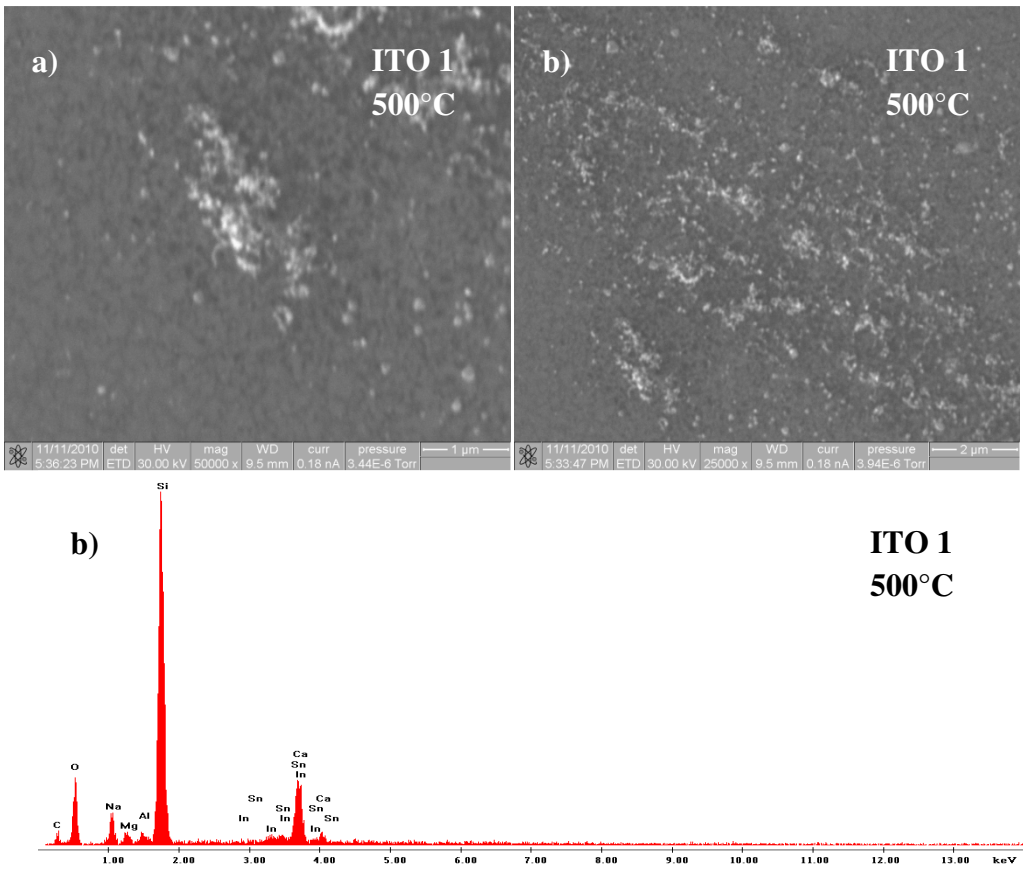

Figure 5.12. a-f) SEM images of CNTs film on ITO 1 surface synthesized with Argon flux of 150sccm and Acetylene flux at 15sccm. CNTs growth time 15 minutes at 500°C. g) EDX analysis of the substrate.

ITO 1 is the best substrate for the proposed organic solar cell. Figure 5.12 reports a graph with all the Transmittance values as function of the wavelengths in the visible light spectrum for ITO 1 substrate. Transmittance is the fraction of incident light at a specified wavelength that passes through a sample.

It can be seen thatITO 5 transmittance is the lowest value due to ITO 5 opaque surface resulting from the CVD process as shown in Figure 5.13.

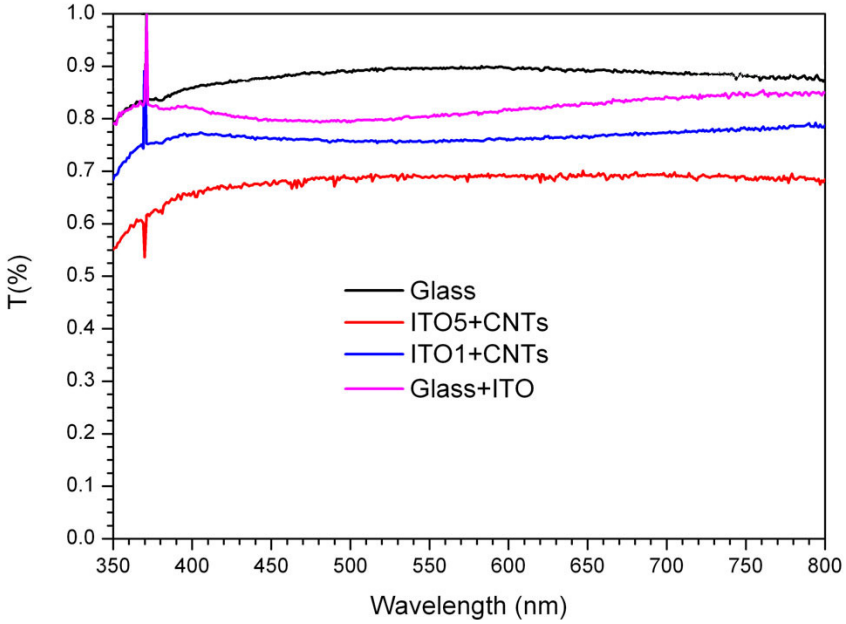

Figure 5.13. Glass, ITO 5, ITO 1 and pure ITO transmittance as function of the wavelengths of the visible light spectrum.

Figure 5.13 shows that ITO1 sample with CNT keeps a good transmittance value, just 5% less than untreated ITO/glass. It is interesting to note that the curves for CNT coatings in the visible light spectrum are almost constant in all the range.

5.2 ORGANIC SOLAR CELL

This paragraph presents the results obtained by A.Capasso and Dr. L Salamandra in the CHOSE laboratories of University of Roma Tor Vergata, which are in the process of being published. All the most important characteristic and measure are also presented for ITO 1, the selected substrate to be used as the transparent electrode for the proposed organic solar cell. The parameters are:

- Work Function:
- V_{OC}:
- I_{SC};
- FF (Fill Factor);

- Efficiency.

Parameters as V_{OC}, I_{SC}, FF and Efficiency are presented in Table 5.4 in order to characterize and understand the behaviour of the organic solar cell. The same parameters for ITO + Pedot (the scheme relative to this cell structure is shown in Figure 5.14) and pure ITO are presented in the same Table 5.4; therefore it is possible to compare all the measures done and highlight the differences.

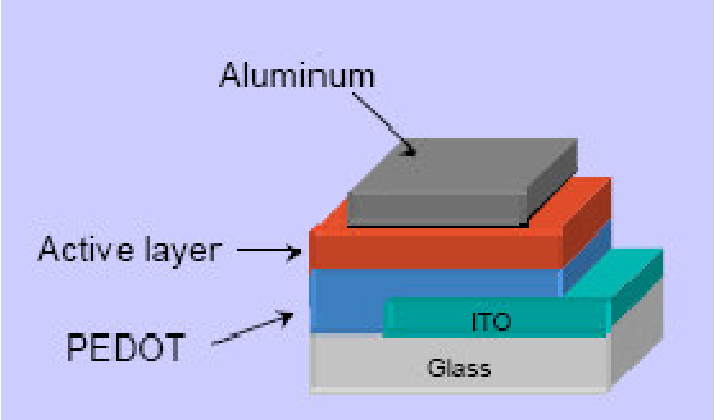

Figure 5.14. Schematic structure for the ITO + PEDOT solar cell.

Table 5.4. VOC, ISC, FF and Efficiency measures for the three different electrodes.

Solar Cell Electrode	V_{OC} [V]	I_{SC} [mA/cm^2]	FF [%]	Efficiency [%]
ITO + PEDOT	4.8	2.1	24.5	0.25
Pure ITO	0.1	1.3	23	0.03
ITO 1 (ITO+CNTs)	0.14	1.7	24	0.055

From equation (1.1) it is possible to obtain the efficiency values for the three different electrodes used in the organic solar cell. The first solar cell built is the standard one with ITO + Pedot as the transparent electrode; the efficiency value is 0.25% for this one.

Pure ITO and ITO + CNTs are used in order to investigate the behaviour of the solar cell without Pedot. The solar cell with ITO + CNTs presents an efficiency value of 0.055% instead of 0.03% given by the one with pure ITO as the transparent electrode. The efficiency of the solar cell with ITO 1 + CNTs made in our laboratories in QUT is almost the double of the pure ITO 1 solar cell efficiency. This result justifies all the strains and experiments done under this project and encourages the experimental research on CNTs used for electronic and photovoltaic applications.

The following Figure 5.15 shows images of the real final solar cell built in Roma Tor Vergata laboratories.

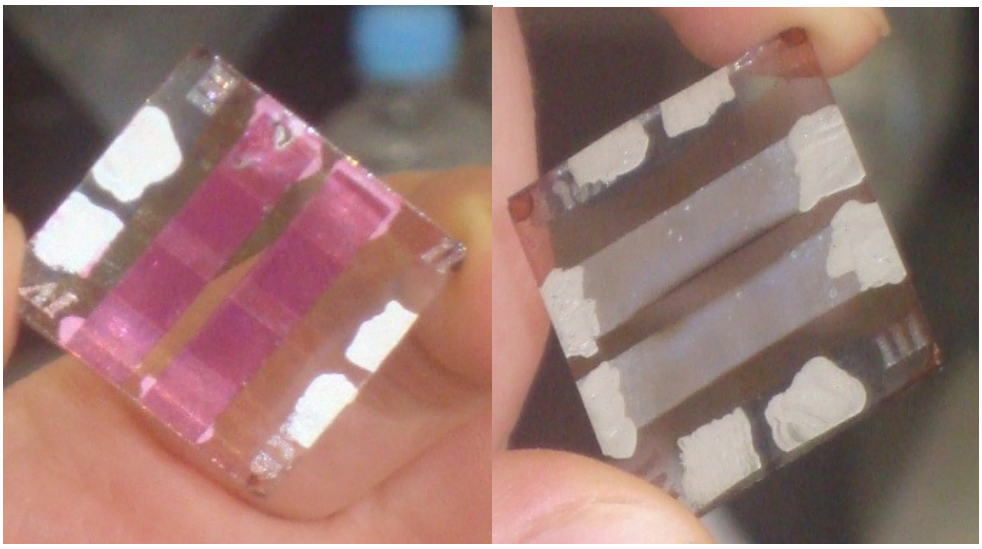

Figure 5.15. Image of the real solar cell built in Roma Tor Vergata laboratories.

6 CONCLUSION

This chapter summarizes the purpose of the master project showing the framework of the entire work. It is given an overview over the experimental results obtained and the direction for future studies as a consequence of this work.

6.1 CONCLUSION

This work is a report of the research activities conducted at the Queensland University of Technology in the field of organic materials for Photovoltaics. In particular, the focus has been on the synthesis of carbon nanotubes by CVD on the transparent metal-oxide electrode (Indium-Tin Oxide) currently used in the organic cell architecture. The design of the CVD parameters and procedures investigated in this study are based upon the previous knowledge acquired through extensive research and findings in QUT. A thorough review of the scientific background concerning organic photovoltaics has been conducted, in order to acquire a sound understanding of the research topic.

In this master project, various sets of CVD parameters are discussed, which can allow to grow an array of MWCNTs on ITO with the desired properties of transparency and electrical conductivity. To this extent, it has been developed a set of CVD synthesis parameters by which it is possible to create a CNT film with low density of tubes, shorter than 200nm. These two characteristics are meant to keep the transparency of the electrode and to avoid the extension of the CNTs over the active layer of the cell. Parameters as Ni and Fe with different deposition thicknesses, gas sources with different flow rates, distinct values of growth temperatures and times have been varied in order to find the optimum CNTs growth. The best result from all the experimental trials is the sample ITO 1. The CVD conditions are the following: a 3 nm thick layer of Fe; 150sccm of Hydrogen and 15sccm of Acetylene; a growth temperature of 500°C and 15 minutes of duration. ITO 1 shows a sufficiently low value of resistance of 300Ω, not exceedingly higher than the pre-growth one (60Ω).

ITO 1 has then been the substrate selected (ITO + CNTs) to be used as transparent electrode in the organic cell test. In the framework of collaboration between QUT and University of Tor Vergata laboratories, the cell have been realized in Tor Vergata laboratories by Dr L. Salamandra and MSc Andrea Capasso. The IV characteristic of the cell has also been measured in Tor Vergata

and shows promising results. The created solar cell outperforms the reference cell, made of an un-treated ITO electrode, in both short circuit current and efficiency. In particular, the efficiency figure for the cell made with ITO 1 is 0.055% while the reference cell only reaches 0.03%.

6.2 SUGGESTION FOR FUTURE DEVELOPMENTS

At this stage, it is now possible to synthesize a MWCNT carpet on ITO substrates coated with iron catalyst film via the synthesis parameters and procedures developed in this project. Although a great deal of work has been done, the growth of vertically-aligned carbon nanotubes (VA-CNTs) still remains a challenge yet to be met. To date, as the mechanisms of CVD growth are not yet fully understood, the high degree of control on CNTs production represents by far the most significant obstacle to the use of nanotubes in photovoltaic applications; an higher control on CNTs production should guarantee the achieving of better efficiencies for organic solar cells.

Accordingly, the future work would be:

- Further studies on the optimum synthesis parameters and techniques in order to effectively synthesize ordered array of short vertically-aligned carbon nanotubes (VA-CNTs), as shown in Figure 6.1, with a controlled density and with specific relative distance on the substrate for photovoltaic applications.
- Investigation and exploitation of the effect of patterning substrate via Focused Ion Beam (FIB); in fact beside the orientation of CNTs on different substrates, their placement is perhaps another important prerequisite towards future applications in nanoelectronics. Patterning is a technique in which nano-sized templates are mechanically scratched on the substrate through FIB before CVD process. In this way it should be possible to grow CNTs onto the substrate without pre-deposition of metal catalyst.

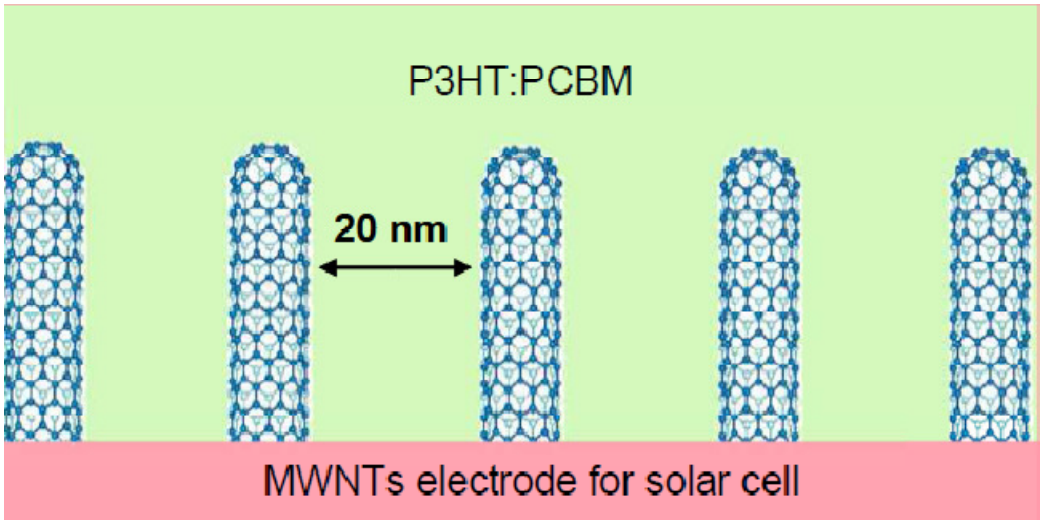

Figure 6.1. Schematic representation of Vertical-Aligned CNTs (VA-CNTs) in an organic solar cell with P3HT-PCBM as the active layer.

Bibliography

1. International Energy Outlook 2009 (May 2009) Energy Information Administration Office of Integrated Analysis and Forecasting, U.S. Department of Energy, Washington, DC 20585.

2. *Basic Research needs for solar energy utilization Report on the Basic Energy Sciences Workshop on Solar Energy Utilization*. 2005: Office of Science U.S. Department of Energy.

3. Surek, T., *Crystal growth and materials research in photovoltaics: progress and challenges.* Journal of Crystal Growth, 2005.

4. Goswami Y., *Solar Energy – Our Future?* , QUT – AIE Public Lecture, 2010.

5. Morton, O., *Solar energy: A new day dawning?: Silicon Valley sunrise.* Nature, 2006.

6. Solar Photovoltaic Cell/Module Manufacturing Activities 2007 Energy Information Administration Office of Integrated Analysis and Forecasting, U.S. Department of Energy, Washington, DC 20585.

7. van Sark, W.G.J.H.M., et al., *Analysis of the silicon market: Will thin films profit?* Energy Policy, 2007.

8. Swanson, R.M., *A vision for crystalline silicon photovoltaics.* Progress in Photovoltaics: Research and Applications, 2006.

9. http://www.physorg.com/news10661.html.

10. Schaefer, H. and G. Hagedorn, *Hidden energy and correlated environmental characteristics of P.V. power generation.* Renewable Energy, 1992.

11. Kato, K., A. Murata, and K. Sakuta, *Energy pay-back time and life-cycle emission of residential PV power system with silicon PV module.* Progress in Photovoltaics: Research and Applications, 1998.

12. Pearce, J. and A. Lau, *Net energy analysis for sustainable energy production from silicon based solar cells.* http://jupiter.clarion.edu/~jpearce/Papers/netenergy.pdf. Copyright by ASME, 2002.

13. Sun, S.-S. and N.S. Sariciftci, *Organic photovoltaics mechanism, materials, and devices*. 2005, Boca Raton, FL : Taylor & Francis.

14. Martin A. Green, K.E.Y.H.W.W., *SHORT COMMUNICATION Solar cell efficiency tables (version 30)*. 2007.

15. O'Regan, B. and M. Gratzel, *A low-cost, high-efficiency solar cell based on dye-sensitized colloidal TiO2 films.* Nature, 1991.

16. Brabec, C.J., N.S. Sariciftci, and J.C. Hummelen, *Plastic solar cells.* Advanced Functional Materials, 2001.

17. Avouris, P., *Carbon nanotube electronics*. Chemical Physics, 2002.

18. Li, G., et al., *High-efficiency solution processable polymer photovoltaic cells by self-organization of polymer blends.* Nature Materials, 2005.

19. Scharber, M.C., et al., *Design rules for donors in bulk-heterojunction solar cells - Towards 10 % energy-conversion efficiency.* Advanced Materials, 2006.

20. Miller, A.J., R.A. Hatton, and S.R.P. Silva, *Interpenetrating multiwall carbon nanotube electrodes for organic solar cells.* Applied Physics Letters, 2006.

21. Ijima, S., *Helical microtubules of graphitic carbon*. Nature, 1991.

22. O'Connell M.J., *Carbon Nanotub*es. Taylor And Francis.

23. Strock, M. *Allotropes of carbon*, 2006. Avalaible from: www.wikipedia.com

24. Geim, A. K. and Novoselov, K. S. (2007). *"The rise of grapheme"*. Nature Materials.

25. Iijima, S., et al., *Structural flexibility of carbon nanotubes.* The Journal of Chemical Physics, 1996.

26. Kim, P., et al., *Thermal Transport Measurements of Individual Multiwalled Nanotubes.* Physical Review Letters, 2001.

27. Baughman, R.H., et al., *Carbon Nanotube Actuators.* Science, 1999.

28. Ebbesen, T.W., et al., *Electrical conductivity of individual carbon nanotubes.* Nature, 1996.

29. Saito, R., M.S. Dresselhaus, and G. Dresselhaus, *Physical properties of carbon nanotubes*. 1998, London :: Imperial College Press.

30. Yu, M.-F., et al., *Strength and Breaking Mechanism of Multiwalled Carbon Nanotubes Under Tensile Load.* Science, 2000.

31. Dalton, A.B., et al., *Super-tough carbon-nanotube fibres.* Nature, 2003.

32. Venema, L.C., *Electronic structure of carbon nanotubes*. 2000: IOS Press Incorporated.

33. Bethune, D.S., et al., *Cobalt-catalysed growth of carbon nanotubes with single-atomic-layer walls.* Nature, 1993.

34. Bolto, B.A., R. McNeill, and D.E. Weiss, *Electronic Conduction in Polymers. III. Electronic Properties of Polypyrrole.* Australian Journal of Chemistry, 1963.

35. Shirakawa, H., et al., *Synthesis of electrically conducting organic polymers: halogen derivatives of polyacetylene, (CH)x.* Journal of the Chemical Society: Chemical Communications, 1977.

36. Roncali, J., *Conjugated poly(thiophenes): synthesis, functionalization, and applications.* Chemical Reviews, 2002.

37. Naarmann, H., *"Polymers, Electrically Conducting".* in Ullmann's Encyclopedia of Industrial Chemistry 2002 Wiley-VCH, Weinheim.

38. Solar Photovoltaic Cell/Module Manufacturing Activities 2007 Energy Information Administration Office of Integrated Analysis and Forecasting, U.S. Department of Energy, Washington, DC 20585.

39. Moliton, A., *Optoelectronics of molecules and polymers*. 2006, New York ; London :Springer.

40. Brabec, C.J., *Organic photovoltaics: technology and market.* Solar Energy Materials and Solar Cells, 2004.

41. http://www.oe-chemicals.com/dictionaryM-Z.html

42. Yu, G. and A.J. Heeger, *Charge separation and photovoltaic conversion in polymer composites with internal donor/acceptor heterojunctions.* Journal of Applied Physics, 1995.

43. Halls, J.J.M., et al., *Efficient photodiodes from interpenetrating polymer networks.* Nature, 1995.

44. Sariciftci, N.S., et al., *Semiconducting polymer-buckminsterfullerene heterojunctions: Diodes, photodiodes, and photovoltaic cells.* Applied Physics Letters, 1993.

45. Sariciftci, N.S., et al., *Photoinduced Electron Transfer from a Conducting Polymer to Buckminsterfullerene.* Science, 1992.

46. Yu, G., et al., *Polymer Photovoltaic Cells: Enhanced Efficiencies via a Network of Internal Donor-Acceptor Heterojunctions.* Science, 1995.

47. Brabec, C.J., et al., *Tracing photoinduced electron transfer process in conjugated polymer/fullerene bulk heterojunctions in real time.* Chemical Physics Letters, 2001.

48. Peumans, P., A. Yakimov, and S.R. Forrest, *Small molecular weight organic thin-film photodetectors and solar cells.* Journal of Applied Physics, 2003.

49. Mihailetchi, V.D., et al., *Cathode dependence of the open-circuit voltage of polymer:fullerene bulk heterojunction solar cells.* Journal of Applied Physics, 2003.

50. Brabec, C.J., N.S. Sariciftci, and J.C. Hummelen, *Plastic solar cells.* Advanced Functional Materials, 2001.

51. Brabec, C.J., et al., *Origin of the Open Circuit Voltage of Plastic Solar Cells.* Advanced Functional Materials, 2001.

52. Koster, L.J.A., et al., *Light intensity dependence of open-circuit voltage of polymer : fullerene solar cells.* Applied Physics Letters, 2005.

53. Scharber, M.C., et al., *Design rules for donors in bulk-heterojunction solar cells - Towards 10 % energy-conversion efficiency.* Advanced Materials, 2006.

54. Nalwa, H.S., *Handbook of Organic Conductive Molecules and Polymers*. Vol. Volume 3. 1997, New York: ohn Wiley and Sons.

55. Lan J.H., Kanicki J., *ITO surface ball formation induced by atomic hydrogen in PECVD and HW-CVD tools*, 1997, University of Michigan.